中国科学: 地球科学 2016 年 第 46 卷 第 6 期: 857 ~ 869
SCIENTIA SINICA Terrae earthcn.scichina.com
《中国科学》杂志社
SCIENCE CHINA PRESS

论 文

金红石 Hf 同位素激光原位多接收等离子体质谱(LA-MC-ICP-MS)测定

李杨[①②], 杨岳衡[①*], 焦淑娟[①], 吴福元[①], 杨进辉[①], 谢烈文[①], 黄超[①]

① 中国科学院地质与地球物理研究所, 岩石圈演化国家重点实验室, 北京 100029;
② 中国科学院大学地球科学学院, 北京 100049
* 通讯作者, E-mail: yangyueheng@mail.iggcas.ac.cn

收稿日期: 2015-09-05; 接受日期: 2015-12-20; 网络版发表日期: 2016-05-23
国家自然科学基金项目(批准号: 41130313, 41525012)资助

摘要 近 20 年来, 激光原位测定技术已广泛应用于锆石、斜锆石、钙钛锆石、异性石等 Hf 含量较高矿物的 Hf 同位素测定上, 但对于 Hf 含量较低(通常<100ppm)矿物的 Hf 同位素激光原位测定, 无论是技术研发还是实际应用, 均开展得较少. 本文利用配有 193nm 激光的 Neptune 多接收等离子体质谱(MC-ICP-MS), 在原位模式下对金红石进行了 Hf 同位素测定实验. 首先, 对国内 U-Pb 年龄参考金红石 JDX 进行了一系列 Hf 同位素测定实验, 确认其 Hf 同位素组成在空间上极为均匀, 溶液测定结果显示, JDX 的 $^{176}Hf/^{177}Hf$ 比值为(0.281795±0.000015) (2SD, n=33), $^{176}Lu/^{177}Hf$ 比值为(0.000018±0.000004) (2SD, n=17). 以 JDX 作为 Hf 同位素测定的内部标准, 对目前金红石微区 U-Pb 年龄其他标准参考物质 R10、Sugluk-4 和 PCA-S207 进行了 $^{176}Hf/^{177}Hf$ 比值测定, 其结果与文献报道值一致. 因此, 对于低 Hf 含量(~50ppm)的金红石, 激光原位多接收等离子体质谱(LA-MC-ICP-MS)可以获得可靠的 $^{176}Hf/^{177}Hf$ 比值, 同时也表明本文所采用的分析方法是合适的. 运用上述建立的方法, 对华北克拉通西部孔兹岩带中不同地区超高温麻粒岩的金红石和锆石进行了 Hf 同位素测定, 结果表明该麻粒岩的变质演化历史比以前认为的要复杂得多.

关键词 金红石, Hf同位素, 激光原位, 多接收等离子体质谱, 孔兹岩

1 引言

金红石是一种广泛分布于火成岩、沉积岩和变质岩中的副矿物. 特别是在镁铁质变质岩中, 金红石的出现与许多特定的变质反应相关, 是绿片岩、榴辉岩和麻粒岩等岩石的标志性矿物之一(Meinhold, 2010). 金红石一般具有较高的U含量, 可用以进行U-Pb定年, 是目前地质年代学研究的重要对象(Vry和Baker, 2006; Li等, 2011a; 李秋立等, 2013; Bracciali等, 2013). 此外, 金红石具有较为特殊的微量元素组成,

中文引用格式: 李杨, 杨岳衡, 焦淑娟, 吴福元, 杨进辉, 谢烈文, 黄超. 2016. 金红石 Hf 同位素激光原位多接收等离子体质谱(LA-MC-ICP-MS)测定. 中国科学: 地球科学, 46: 857–869, doi: 10.1360/N072015-00087
英文引用格式: Li Y, Yang Y H, Jiao S J, Wu F Y, Yang J H, Xie L W, Huang C. 2015. *In situ* determination of hafnium isotopes from rutile using LA-MC-ICP-MS. Science China Earth Sciences, 58: 2134–2144, doi: 10.1007/s11430-015-5215-2

尤其是Nb和Ta等高场强元素的重要载体, 是沉积岩源区示踪的重要对象(Zack等, 2002, 2004b; Luvizotto等, 2009). 同时, 金红石Zr的含量与温度相关, 金红石的Zr温度计可为我们反演地质演化过程提供重要信息(Zack等, 2004a; Watson等, 2006; Cherniak等, 2007; Ferry和Watson, 2007; Tomkins等, 2007; Ewing等, 2013). 在这一基础上, 人们开始探索金红石Hf同位素测定的可能性(Choukroun等, 2005; Morisset等, 2014), 以期建立与锆石类似的金红石U-Pb年龄、微量元素、形成温度和Hf同位素组成示踪地质演化历史的研究体系(Ewing等, 2011). 更为重要的是, 含金红石的岩石还经常出现锆石. 这样, 金红石和锆石两矿物的U-Pb年龄、微量元素、形成温度和Hf同位素组成将为地质历史过程的精细刻画提供前所未有的重要信息(Ewing等, 2014).

但是, 相对目前较为成熟的锆石Hf同位素测定而言, 金红石Hf同位素的激光原位测定具有相当的挑战性. 主要原因有: 第一, 缺乏基体匹配的Hf同位素测定标准. 或者说, 现在还不能断定, 是否可以用锆石等矿物来做金红石Hf同位素测定的外部标准. 第二, 金红石Hf含量通常较低(一般<50ppm), 而低的Hf含量使得测定信号强度较低, 影响数据的质量. 另外值得注意的是, 金红石同样具有极低的Yb和Lu含量, 这一特点虽然使得我们难以获得准确的校正干扰系数, 却也暗示金红石可能无需进行Yb和Lu的干扰校正, 但是由低含量Yb和Lu引起的Hf同位素测试结果的不确定度究竟有多大, 目前尚无定论. 尽管部分国外学者目前已对这一问题进行了有益的探索和尝试, 并显示了这一技术潜在的应用价值, 但由于该方法的研发还处在初步发展阶段, 许多重要问题仍有待解决(Choukroun等, 2005; Aulbach等, 2008; Ewing等, 2011).

在这一背景下, 本文采用配有193nm激光的Neptune MC-ICP-MS仪器, 建立了金红石激光原位Hf同位素测定技术. 在研发出内部标准的基础上, 我们对目前原位微区U-Pb定年工作中的若干金红石标准进行了Hf同位素比值测定, 获得了与溶液一致的$^{176}Hf/^{177}Hf$组成. 在此基础上, 我们对华北克拉通西部孔兹岩中的金红石进行了Hf同位素测定, 结合其微量元素和U-Pb年龄信息, 获得了一些新认识, 展示了金红石激光原位Hf同位素测定技术的应用前景.

2 金红石 U-Pb 参考标准物质简介

本文开展Hf同位素工作的金红石是国内外微区原位U-Pb年代学常用的参考物质. JDX是一颗5cm×5cm×2.5cm的自形金红石粗晶, 具体产地不明, 系中国科学院地质与地球物理研究所SIMS实验室研发的U-Pb年代学监测标样, 其$^{206}Pb/^{238}U$加权平均年龄为(509±8)Ma (Li等, 2011a)(图1a). R10是一颗来自挪威南部Gjerstd地区的厘米级单颗粒金红石(Luvizotto等, 2009)(图1b). Sugluk-4是来自加拿大跨哈德逊造山带Ungava地区的麻粒岩相石英岩中的金红石, 颗粒大小在100~500μm之间, 呈红褐色半透明状, 晶体为自形-半自形结构(图1c) (Bracciali等, 2013). PCA-S207是来自加拿大Athabasca地区麻粒岩相副片麻岩中的金红石, 颗粒大小从数十微米到数百微米不等, 颜色从红褐至深褐色, 晶体主要为他形结构(图1d) (Bracciali等, 2013). 表1是这些金红石U-Pb参考标准物质的相关微量元素组成情况. 从该表可以看出, 金红石的Hf含量大多<50ppm, 且其Lu和Yb含量极低. 除R10金红石外, 目前还没有其他金红石Hf同位素的报道(Luvizotto等, 2009).

3 实验方法

金红石原位Hf同位素测定在中国科学院地质与地球物理研究所Neptune MC-ICP-MS和GeoLas Pro型193 nm准分子激光剥蚀系统上进行. 有关仪器的基本情况详见文献Wu等(2006)和谢烈文等(2008).

本文金红石激光原位Hf同位素测定的样品制备类似于锆石Hf同位素激光分析, 将待测定的天然金红石颗粒用双面胶粘在载玻片上, 放上PVC环, 将环氧树脂和固化剂进行充分混合后注入PVC环中, 待树脂充分固化后将样品座从载玻片上剥离, 并对其进行抛光, 直到样品露出一个光滑的平面. 样品测试之前用稀硝酸超声清洗待测靶, 用酒精轻擦样品表面, 以除去可能的污染.

激光金红石Hf同位素分析与激光测定锆石(斜锆石)Hf同位素分析非常相似(Wu等, 2006; 谢烈文等, 2008), 典型仪器参数和法拉第杯结构见表2. 激光剥蚀的斑束直径为60、90、120和160μm, 频率为20Hz, 采样方式为单点剥蚀. 以He作为剥蚀物质的载气,

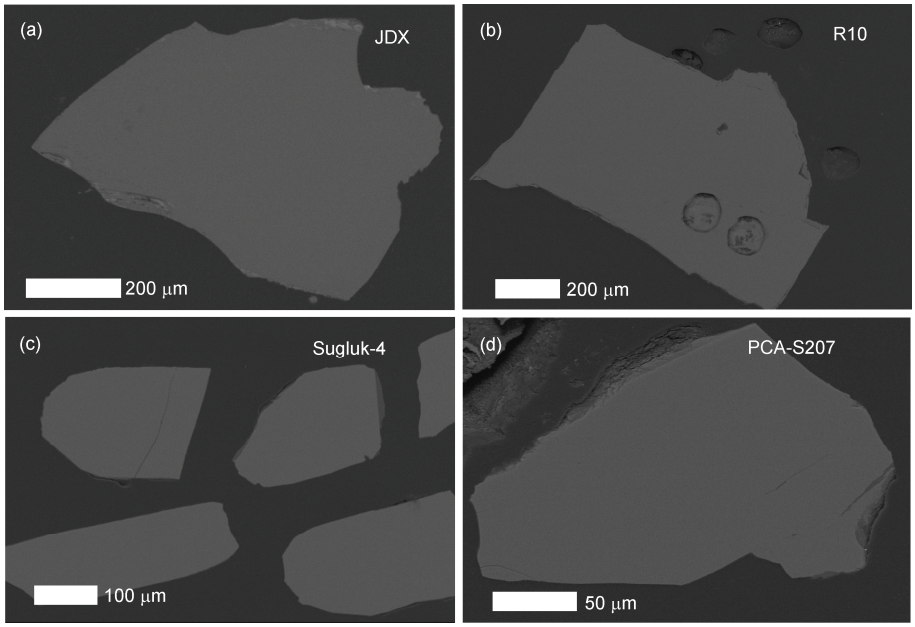

图 1　金红石参考标准物质 JDX、R10、Sugluk-4 和 PCA-S207 背散射照片

表 1　金红石 U-Pb 参考标准物质的相关微量元素(单位: ppm)

	JDX [a)]	R10 [b)]	Sugluk-4 [c)]	PCA-S207 [c)]
Zr	308	778	836	977
Nb	337	2659	1461	1265
Yb	0.015			
Lu	0.0064	0.041		
Hf	50	38	51	37
Ta	64	480	105	46
W		108	221	18
Pb	0.52	0.081	16	8
Th	0.005	<0.004		
U	1.1	44.1	59.5	22.8

a) 本文数据; b) Luvizotto等(2009); c) Bracciali等(2013)

将激光剥蚀的物质送入Neptune MC-ICP-MS进行Hf同位素测定.

3.1　溶液测定

金红石溶液测试主要包括样品溶解、化学分离和质谱测试. 准确称量约50mg金红石粉末至容积为10mL高压溶样弹中, 加适量的^{176}Lu-^{180}Hf稀释剂和HF-HNO_3-$HClO_4$ (2mL-1mL-0.1mL), 然后放入烘箱加热至190℃保温7天, 冷却后置于电热板上赶尽HF和$HClO_4$, 最后加入5mL 3mol/L HCl在电热板上100℃保温12h, 准备化学分离. Lu和Hf分离是通过Ln树脂完成, 首先用3mol/L HCl淋洗基体元素和轻-中稀土元素, 用4mol/L HCl淋洗并接收Lu, 用6mol/L HCl淋洗以除去残余Yb和Lu, 然后用4mol/L HCl+0.5% H_2O_2淋洗Ti, 直至淋洗液无色, 最后用2mol/L HF淋洗并接收Hf、Lu和Hf组分待蒸干后用2% HNO_3提取至离心管待测. 有关化学分离与质谱测试详细过程参见文献Yang等(2010).

实际样品测试前, 我们用200ppb Alfa Hf标准溶液调试Neptune MC-ICP-MS获得最佳的信号强度和平顶峰, 然后用50ppb的JMC475标准溶液来检测仪器测试结果的准确性和稳定性. 如图2所示, 我们15次测定的加权平均值为(0.282172±0.000029) (2SD, n=15), 该测定值与文献报道的结果在误差范围内一致(Nowell等, 1998).

3.2　激光测定

3.2.1　JDX 金红石 Hf 同位素均匀性检验

尽管国内外同行已经研发了一些金红石U-Pb年代学标准参考物质(Luvizotto等, 2009; Li等, 2011a; Bracciali等, 2013), 但是到目前为止, 还没有大家公认的金红石Hf同位素标准物质. 除了R10金红石外, 也没有其他金红石的Hf同位素报道(Luvizotto等, 2009).

表 2　典型的仪器参数和法拉第杯结构

Neptune MC-ICP-MS					激光剥蚀系统			
RF功率		1250W			仪器型号		GeoLas Pro	
冷却气流量		16L/min			激光波长		UV 193nm	
辅助气流量		0.8L/min			能量密度		12J/cm^2	
提取电压		–2000V			束斑大小(μm)		60、90、120、160	
聚焦电压		–645V			激光频率		20Hz	
分辨率		~400			载气流量		0.83L/min	
采样模式(溶液)		9 blocks of 10 cycles						
采样模式(激光)		1 block of 200 cycles						
积分时间		4.194s (溶液) 或 0.262s (激光)						
Hf杯结构								
法拉第杯	L4	L3	L2	L1	Center	H1	H2	H3
质量数	172	173	175	176	177	178	179	180
同位素	Yb	Yb	Lu	Hf+Yb+Lu	Hf	Hf	Hf	Hf

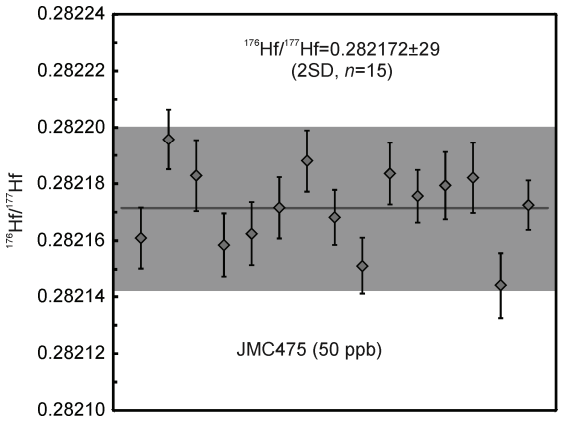

图 2　50 ppb 的 JMC475 Hf 标准溶液监测仪器稳定性

灰色线段为加权平均值

本文首先对我所离子探针实验室的U-Pb年代学标准物质JDX进行其Lu-Hf同位素组成的溶液定值. 如图3所示, 在不同时间段, 我们对12份JDX颗粒进行了多次重复Lu、Hf含量和Hf同位素比值测定实验. JDX的Hf含量(50.1±0.7)ppm (2SD, n=17), Lu含量(0.0064±0.0014)ppm (2SD, n=17), ^{176}Lu/^{177}Hf=(0.000018±0.000004) (2SD, n=17), ^{176}Hf/^{177}Hf=(0.281795±0.000015) (2SD, n=33).

用溶液法获得了准确的JDX的Hf同位素组成后, 我们把JDX金红石作为实验室的内部标准进行了长期的激光实验测试. 如图4所示, JDX的^{176}Hf/^{177}Hf和^{177}Hf/^{179}Hf比值(未作分馏校正)的长期测试值具有非常窄的变化范围, 表明JDX用来作实验室的Hf同位素内部标准是比较合适的. Li等(2011a)用二次离子探针对JDX的U-Pb体系进行过研究, 发现具有轻微的不谐和, 因此通常作为SIMS金红石U-Pb定年的监控标样. 但是通过本次研究, 发现JDX的Hf含量足够高, 多份溶液分析表明, 其^{176}Hf/^{177}Hf具有很好的一致性, 因此, 我们把JDX作为金红石激光原位Hf同位素的实验室内部标准参考物质.

3.2.2　同质异位素干扰校正

激光原位Hf同位素测定过程中, Hf的干扰主要来自于Yb和Lu, 通常采用监控无干扰的^{173}Yb和^{175}Lu来扣除^{176}Yb和^{176}Lu对^{176}Hf的干扰(Thirlwall和Walder, 1995; Thirlwall和Anczkiewicz, 2004; Wu等, 2006; Yuan等, 2008; Hu等, 2012). 如前所述, 一方面, 因为金红石的Yb和Lu含量极低, 在实际测试过程中可以忽略这些干扰; 另一方面, 考虑到金红石的低Hf含量, 尽管金红石的Yb和Lu含量极低, 我们仍然需要扣除Yb和Lu干扰. 因此, 本次研究工作将比较两者的差异, 评估低含量Yb和Lu对金红石Hf同位素测试结果的影响.

如果进行Yb和Lu的干扰校正, 其原理与锆石Hf同位素测定大致相同(式(1)):

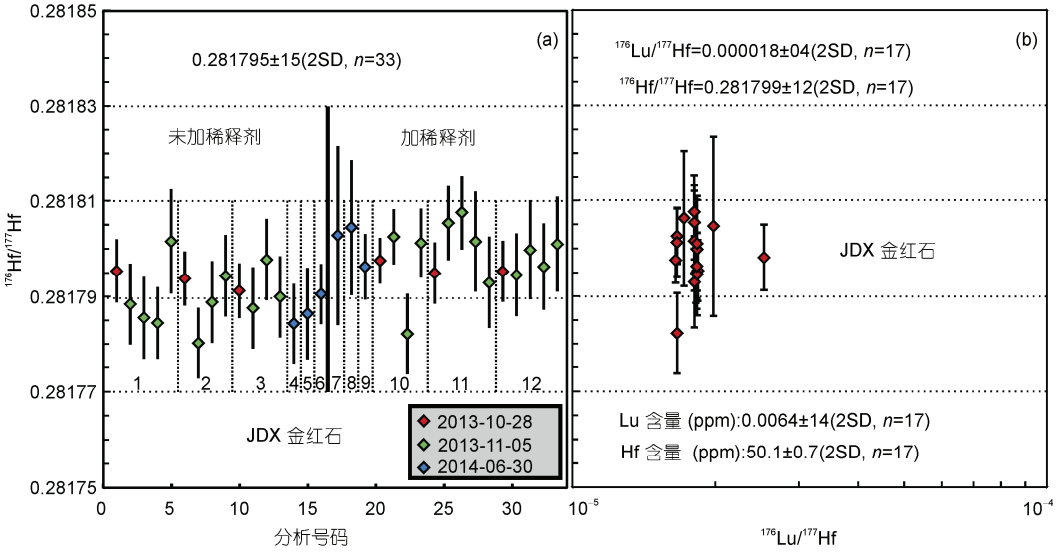

图 3　金红石 JDX 不同时期 Lu-Hf 同位素溶液测试结果

(a) 1~6 份未加稀释剂测定 Hf 同位素组成, 7~12 份加入稀释剂同时获得 Lu、Hf 含量和 Hf 同位素组成; (b) 同位素稀释法获得 JDX 的 Lu-Hf 同位素组成

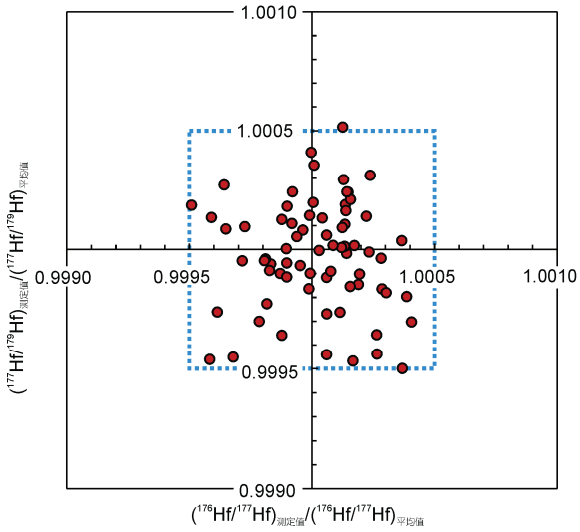

图 4　JDX 参考物质均匀性检验

$$^{176}\mathrm{Hf}=^{176}\mathrm{M}-[^{175}\mathrm{Lu}_m\times(^{176}\mathrm{Lu}/^{175}\mathrm{Lu})_t(\mathrm{M}_{176}/\mathrm{M}_{175})^{\beta\mathrm{Yb}}+^{172}\mathrm{Yb}_m\times(^{176}\mathrm{Yb}/^{172}\mathrm{Yb})_t(\mathrm{M}_{176}/\mathrm{M}_{172})^{\beta\mathrm{Yb}}]. \quad (1)$$

质量歧视校正使用指数法则, Hf的质量歧视因子β_{Hf}根据^{179}Hf/^{177}Hf=0.7325计算. 对于锆石, β_{Yb}利用测定的^{172}Yb和^{173}Yb, 根据^{172}Yb/^{173}Yb=1.35272来计算, 同时因为无法单独计算β_{Lu}, 故而用β_{Yb}来代替β_{Lu}. 对于金红石, 由于Yb的含量很低, 无法根据测量^{172}Yb和^{173}Yb来计算β_{Yb}, 所以我们采用β_{Hf}来代替β_{Yb}和β_{Lu}.

如果不进行Yb和Lu的干扰校正, 则所有176质量数接收的信号都认为是^{176}Hf的信号. 以JDX和R10的15次测试结果为例, 将两种方法的数据结果进行对比, 结果如图5所示: JDX不扣除干扰的^{176}Hf/^{177}Hf比值为(0.28204±0.00019)(2SD), 而进行干扰扣除的^{176}Hf/^{177}Hf比值为(0.28180±0.00013)(2SD); R10不扣除干扰的^{176}Hf/^{177}Hf比值为(0.28262±0.00057)(2SD), 而进行干扰扣除的^{176}Hf/^{177}Hf比值为(0.28219±0.00016)(2SD). 显然, 进行干扰扣除的^{176}Hf/^{177}Hf结果的准确度和精密度都要好于不进行干扰扣除的结果. 这一认识也可以从图6来得到进一步的证明. 本文研究的4个金红石参考物质和锆石标准(Mud Tank和GJ-1), 尽管金红石的Yb和Lu含量低, 但是同一样品有差别, 不同的样品也有差别. 有的金红石样品Yb和Lu的量甚至和锆石Mud Tank的Yb和Lu的量相当, 证实了进行干扰扣除的必要性. 因此, 在我们后续的金红石Hf同位素测试过程中都进行了干扰扣除.

3.2.3　基体效应

与溶液Hf同位素测试不同, 激光原位测定Hf同位素通常需要基体匹配的标准矿物作为标准来监控仪器. 相对目前较为成熟的激光原位锆石Hf同位素测定而言, 金红石Hf同位素的激光原位测定具有相当的困难性. 其主要原因之一就是缺乏基体匹配的

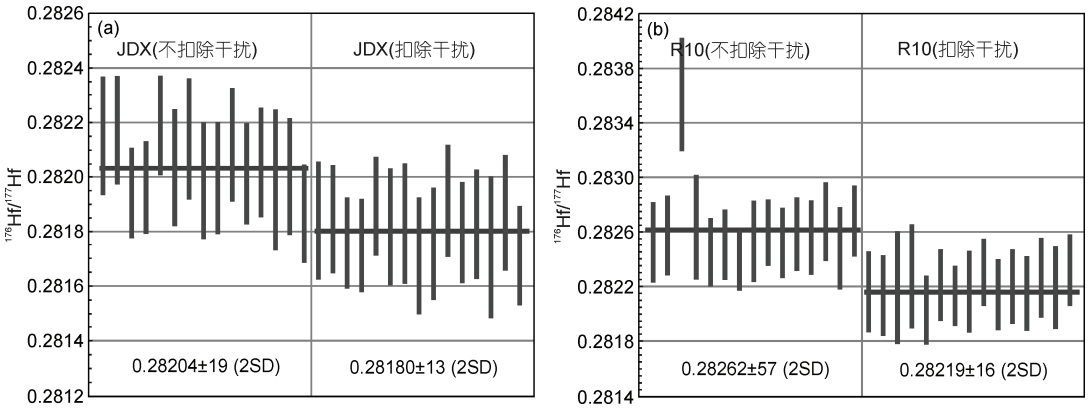

图 5　干扰不扣除和干扰扣除的 JDX 和 R10 的 $^{176}Hf/^{177}Hf$ 结果比较

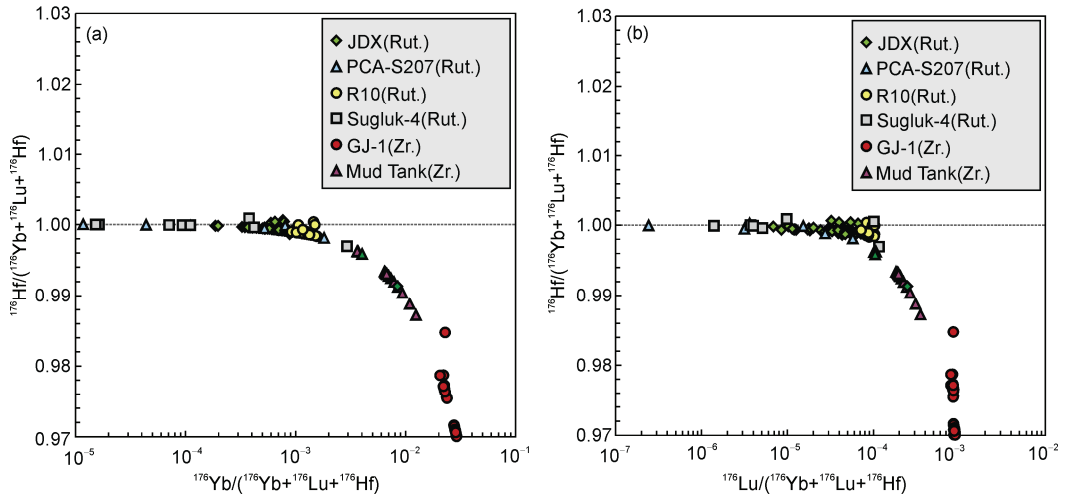

图 6　金红石标准物质(JDX、R10、PCA-S207 和 Sugluk-4)与锆石标准(Mud Tank 和 GJ-1)的 176 质量数的信号强度比

^{176}Hf 的干扰主要来自 ^{176}Yb, 个别金红石样品的 ^{176}Yb 干扰可以与锆石标准 Mud Tank 相当, 说明干扰扣除的必要性

Hf同位素测定标准物质或标准矿物, 或者说, 现在还不能断定, 是否可以用广泛使用的锆石标准矿物(如91500、GJ-1和Mud Tank等)来做金红石Hf同位素测定的外部标准(Choukroun等, 2005; Ewing等, 2011).

首先, 进行相关实验来检验锆石是否能够替代金红石作标准参考物质. 在相同的仪器参数条件下, 以锆石Mud Tank为标准, 同时进行锆石和金红石的Hf同位素测定实验. 如图7所示, 尽管标准锆石GJ-1能够获得可靠的$^{176}Hf/^{177}Hf$比值(图7a), 但是JDX金红石获得的$^{176}Hf/^{177}Hf$与其溶液值存在明显的系统偏差(图7b). 这说明, 不能采用标准锆石作为金红石激光原位Hf同位素测定的标准. 具体原因可能是两个方面, 一是锆石和金红石的组成完全不一样, 导致激光剥蚀和质谱测试中仪器分馏行为差异; 二是锆石Hf含量较高, 通常为上千百万分比浓度(ppm), 而金红石Hf含量只有几十到上百百万分比浓度(ppm), 使得我们很难用相同的激光参数来进行锆石和金红石的Hf同位素测定. 在本文后续工作中, 我们一直使用JDX作为实验室的金红石内部工作标准, 开展相关工作.

4　结果与讨论

4.1　金红石 U-Pb 标准物质的 Hf 同位素组成

R10是一颗来自挪威南部Gjerstd地区的厘米级单颗粒金红石, Luvizotto等(2009)用ID-MC-ICP-MS测量过其Hf含量为(37.4±0.4)ppm(边部)和(38.9±0.4)ppm

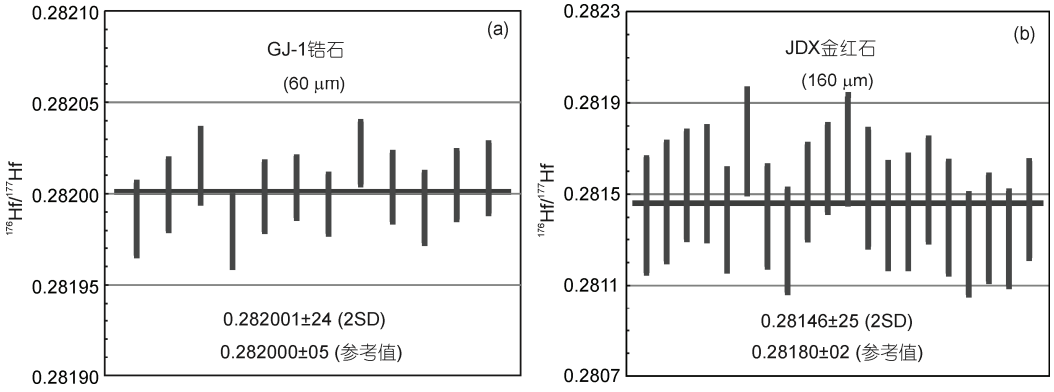

图 7　标准锆石和金红石的激光原位 Hf 同位素测定的基体效应

(核部), 相应的Lu含量分别为(0.0513±0.0005)ppm (边部)和(0.0300±0.0100)ppm(核部), 其$^{176}Hf/^{177}Hf$比值分别为(0.282178±0.000009)(边部)和(0.282178±0.000012)(核部). 本次测试为1.5mm×0.5mm R10碎片(图1b). 在160μm束斑下, 我们42次分析的$^{176}Hf/^{177}Hf$加权平均结果为(0.282157±0.000204)(2SD, *n*=42), 与Luvizotto等(2009)用同位素稀释法获得的(0.282178±0.000012)在误差范围内一致(图8), Ewing等(2011)用233μm激光束斑的测定结果为(0.282199± 0.000280) (2SD, *n*=3).

Sugluk-4是来自加拿大哈德逊造山带Ungava地区的麻粒岩相石英岩中的金红石(图1c), 颗粒大小在100~500μm之间, 呈红褐色半透明状, 晶体为自形-半自形结构. Bracciali等(2013)测定该金红石的Hf含量从36~67ppm, 平均约为51ppm. PCA-S207是来自加拿大Athabasca地区麻粒岩相副片麻岩中的金红石(图1d), 颗粒大小从数十微米到数百微米不等, 颜色从红褐至深褐色, 晶体主要为他形结构. 该金红石的Hf含量从20~60ppm不等, 平均约为37ppm(Bracciali等, 2013). 两者的LA-MC-ICP-MS U-Pb年龄分别为(1719±14)和(1865±7.5)Ma, 目前还没有Hf同位素数据的报道. 在160μm束斑下, 我们对Sugluk-4和PCA-S207的$^{176}Hf/^{177}Hf$进行了15次分析, 结果分别为(0.281172±0.000107) (2SD)和(0.281246±0.000146)(2SD) (图8, 表3).

Bracciali等(2013)曾对金红石R10、Sugluk-4和PCA-S207进行过U-Pb定年工作的测试, 指出R10并不适合做U-Pb定年的参考物质, 而后两者分别可以作为金红石U-Pb定年的第一和第二参考物质(Sugluk-4

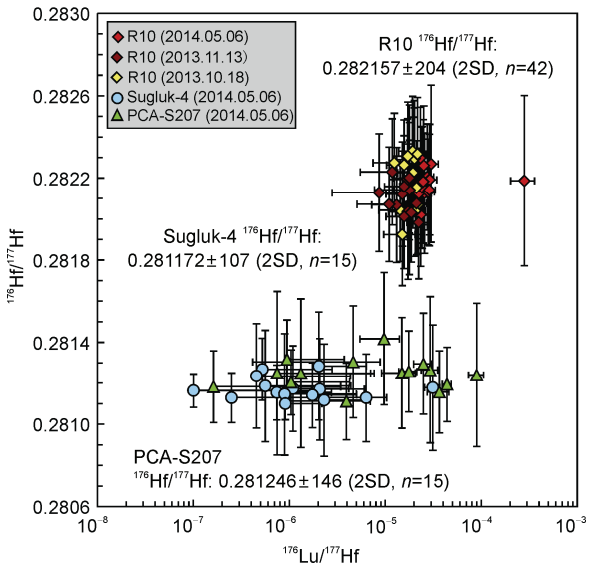

图 8　金红石标准 R10, Sugluk-4 和 PCA-S207 的激光测定 Lu-Hf 同位素结果

的$^{207}Pb/^{206}Pb$和$^{206}Pb/^{238}U$的重现性要略好于PCA-S207). 由微量元素可知, 金红石Sugluk-4的平均Hf含量比PCA-S207更高, 且具有更狭窄的$^{176}Hf/^{177}Hf$比值变化范围, 似乎更适合做Hf同位素标样. 由此看来, 金红石Sugluk-4既能作U-Pb定年标样, 又能够作Hf同位素测定的标样. 但是由于本次测试矿物颗粒有限, 采集的数据较少, 其作为Hf同位素测定标样的可能性还需更多的工作来加以证实.

4.2　激光原位如何准确获得金红石的 Hf 同位素组成

由于金红石的Hf含量较低(~50ppm), 因此在激光剥蚀进样时的Hf信号强度比较弱, 但是究竟Hf信

表 3　金红石 U-Pb 年龄参考物质 Lu-Hf 同位素组成

样品名	$^{176}Yb/^{177}Hf$	2SD	$^{176}Lu/^{177}Hf$	2SD	$^{176}Hf/^{177}Hf$	2SD(*n*=测试次数)	方法	资料来源
JDX			0.000018	0.000004	0.281795	0.000015(*n*=33)	溶液	本文数据
JDX	0.000200	0.000150	0.000009	0.000010	0.281796	0.000187(*n*=89)	激光	本文数据
R10			0.000029	0.000012	0.282199	0.000280(*n*=3)	激光	Ewing等(2011)
R10					0.282178	0.000012(*n*=2)	溶液	Luvizotto等(2009)
R10	0.000379	0.000480	0.000026	0.000081	0.282157	0.000204(*n*=42)	激光	本文数据
Sugluk-4	0.000080	0.000392	0.000003	0.000016	0.281172	0.000107(*n*=15)	激光	本文数据
PCA-S207	0.000647	0.001668	0.000019	0.000049	0.281246	0.000146(*n*=15)	激光	本文数据

号低到什么程度会导致仪器无法准确测量, 我们还不得而知, 也没有任何有关这方面的报道. 基于此, 我们利用不同浓度的JMC475国际标准溶液(50、25、10、5、2.5和1ppb), 在与激光剥蚀相同的数据采集条件下, 用溶液进样方法来模拟激光进样, 结果如图9b所示, 随着溶液浓度逐渐降低, Hf的信号强度也逐渐降低, 当^{176}Hf的信号强度降低到大约10mV的时候所测的$^{176}Hf/^{177}Hf$比值明显地偏离了真实值, 这可能是由于信号太弱, 以至于已经接近法拉第杯的检测极限所造成, 这也可以从我们激光测试实验中得到较好的印证(图9a). 由此, 我们认为, 如果^{176}Hf的信号强度低于10mV, 所测的$^{176}Hf/^{177}Hf$比值会偏离真实值. 为了能够获得可靠的数据, 激光金红石Hf同位素测定过程中, ^{176}Hf的信号强度至少大于10mV. 在实际样品测试中, 我们可以通过改变激光束斑的大小来满足这一条件.

关于激光测定对金红石Hf含量的要求, 我们可以用图10来加以说明, 将我们前面测定的金红石数据总结发现, 不同Hf含量金红石在不同激光束斑直径下获得的数据精度不同. 样品中Hf含量越高, 激光剥蚀束斑直径越大, 所获得的信号越强, 所获得$^{176}Hf/^{177}Hf$比值的精度越高. 如果假设讨论地质问题所要求的误差为±3.5ε单位, 它所对应的$^{176}Hf/^{177}Hf$比值误差为0.0001. 对50ppm Hf含量的金红石, 我们使用150μm束斑, 获得的$^{176}Hf/^{177}Hf$比值误差为0.0002, 而对于大于100ppm Hf含量金红石, 使用150μm的束斑, 获得的$^{176}Hf/^{177}Hf$比值误差都会好于0.0001. 可以相信, 随着技术的发展, 未来激光测定对Hf含量的要求还会有所降低. 因此, 对于大多数金红石样品而言(Hf含量~50ppm), 目前的技术完全可以获得所

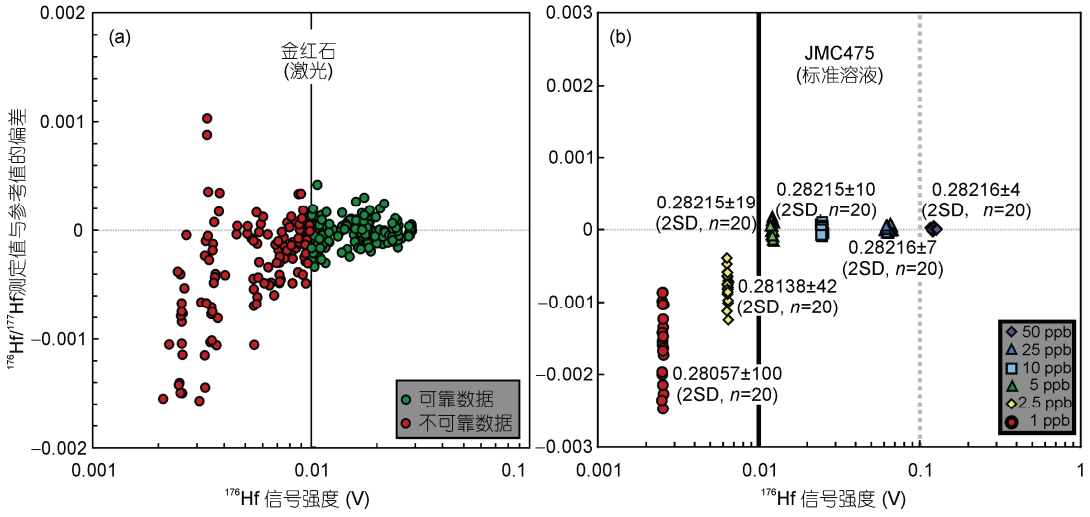

图 9　激光原位准确获得金红石 Hf 同位素的合适实验条件

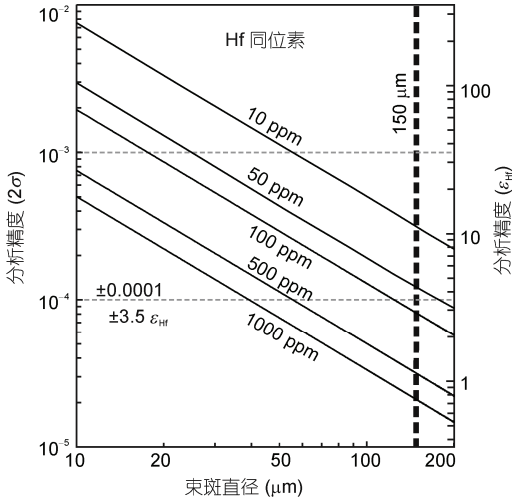

图 10　激光原位测定金红石 Hf 同位素的数据精度与激光参数选择及金红石 Hf 含量之间关系

要求的数据, 这在下面的应用实例中得到了证明.

5　应用实例

位于华北克拉通西部的孔兹岩带是一套主要由长英质副片麻岩、夕线石榴斜长(钾长或二长)片麻岩、长石石英岩、大理岩以及钙硅酸岩等组成的麻粒岩相变沉积岩(即孔兹岩系)夹少量基性麻粒岩(卢良兆等, 1992, 1996; Zhao等, 1999, 2005). 该带近东西向展布, 长约1000km, 自西向东划分为贺兰山-千里山、乌拉山-大青山和集宁-凉城-丰镇三个亚带(图11). 一般认为, 它是由北部的阴山陆块和南部的鄂尔多斯陆块于约1.95 Ga时碰撞而成(赵国春等, 2002; 赵国春, 2009; Zhao等, 2005), 其沉积时代约为1.95~2.00Ga (Xia等, 2006, 2008; Wan等, 2006, 2009). 根据锆石U-Pb定年, 这些孔兹岩系一般保留了1.97~1.94和1.87~1.82Ga两期变质作用(Yin等, 2009, 2011; Zhao等, 2010; Li等, 2011b; 董春艳等, 2012; Ma等, 2012; Liu等, 2013; Jiao等, 2013). 目前的研究显示, 1.97~1.94Ga变质可能与阴山-鄂尔多斯块体的碰撞有关, 而1.87~1.82Ga的变质作用可能与华北克拉通东西陆块的拼合有关或代表了造山后的伸展事件(Zhao等, 2005, 2012; Jiao等, 2013; Peng等, 2014). 此外, 本区还发育1.92~1.91Ga的超高温麻粒岩, 推测可能与地幔岩浆的注入加热有关(Santosh等, 2007, 2009;

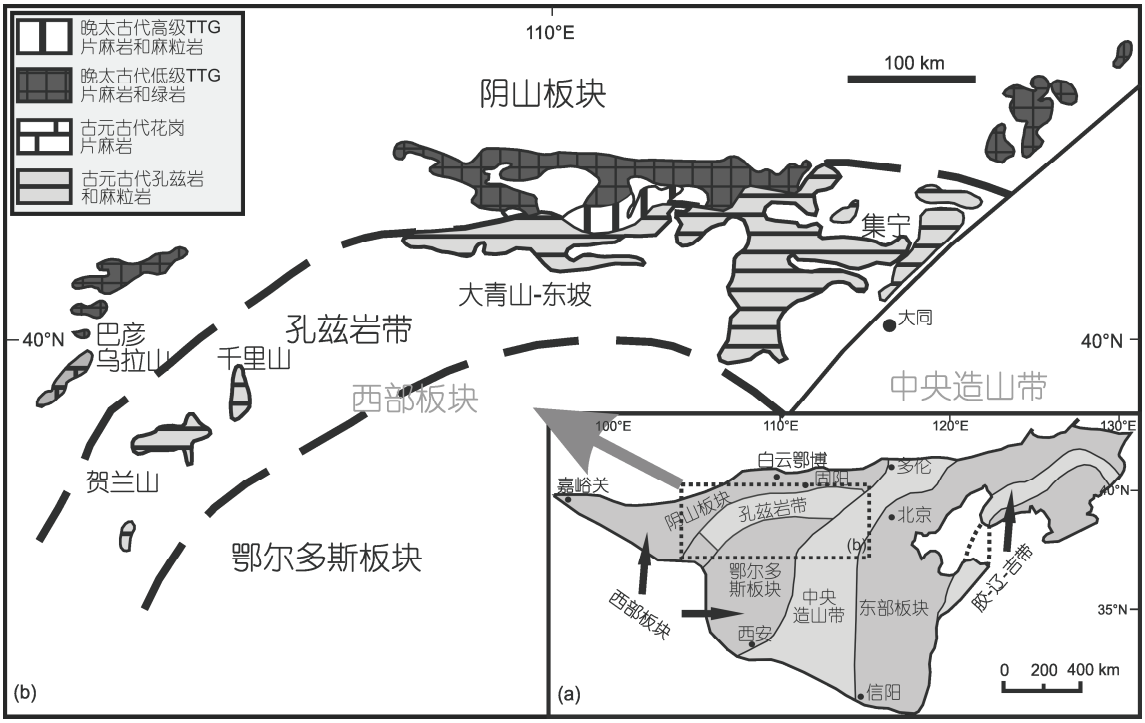

图 11　华北克拉通构造区域划分图(a)和西部板块内部孔兹岩带的地质单元简图(b)

据 Dan 等(2012)修改

Guo等, 2012).

我们对上述孔兹岩带中大青山和集宁地区的麻粒岩进行了系统采样, 并分离出其中的金红石和锆石进行U-Pb年龄与Hf同位素测定(表4, 图12). 研究表明, 这两地的麻粒岩都经历了高温甚至超高温变质作用, 部分样品发育假蓝宝石(Jiao和Guo, 2011;

表 4　华北克拉通西部陆块的孔兹岩带中锆石和金红石 U-Pb 年龄和 Hf 同位素组成

样品名	矿物	年龄(Ma)	$^{176}Yb/^{177}Hf$	$^{176}Lu/^{177}Hf$	$^{176}Hf/^{177}Hf$	2SE(n=测试次数)	$\varepsilon_{Hf}(1780)$	2σ	方法
大青山-东坡地区									
09DP14	锆石	1842±8	0.00067	0.000021	0.281474	0.000009 (n=16)	−6.28	0.45	激光
	金红石	1734±11	0.00000	0.000000	0.281531	0.000014 (n=15)	−4.23	0.70	激光
	金红石				0.281539	0.000003 (n=7)			溶液
08JDP05	金红石		0.00029	0.000001	0.281560	0.000036 (n=4)	−3.20	1.30	激光
	金红石				0.281555	0.000005 (n=2)			溶液
08JDP06	金红石		0.00070	0.000004	0.281541	0.000047 (n=2)	−3.88	1.68	激光
	金红石				0.281554	0.000010 (n=2)			溶液
集宁-土贵乌拉地区									
09TGS11	锆石	1843±8	0.00081	0.000023	0.281484	0.000008 (n=16)	−5.93	0.50	激光
	金红石	1780±6	0.00011	0.000003	0.281593	0.000015 (n=15)	−2.03	0.60	激光
	金红石				0.281591	0.000011 (n=4)			溶液
09TGS38	锆石	1944±8	0.00068	0.000020	0.281580	0.000010 (n=16)	−2.51	0.65	激光
	金红石	1783±5	0.00003	0.000002	0.281598	0.000012 (n=15)	−1.85	0.48	激光
	金红石				0.281605	0.000008 (n=7)			溶液
08TG13	金红石		0.00001	0.000001	0.281600	0.000014 (n=15)	−1.78	0.55	激光
	金红石				0.281602	0.000009 (n=4)			溶液
08TPS01	金红石		0.00003	0.000000	0.281597	0.000012 (n=15)	−1.89	0.48	激光
	金红石				0.281597	0.000015 (n=4)			溶液

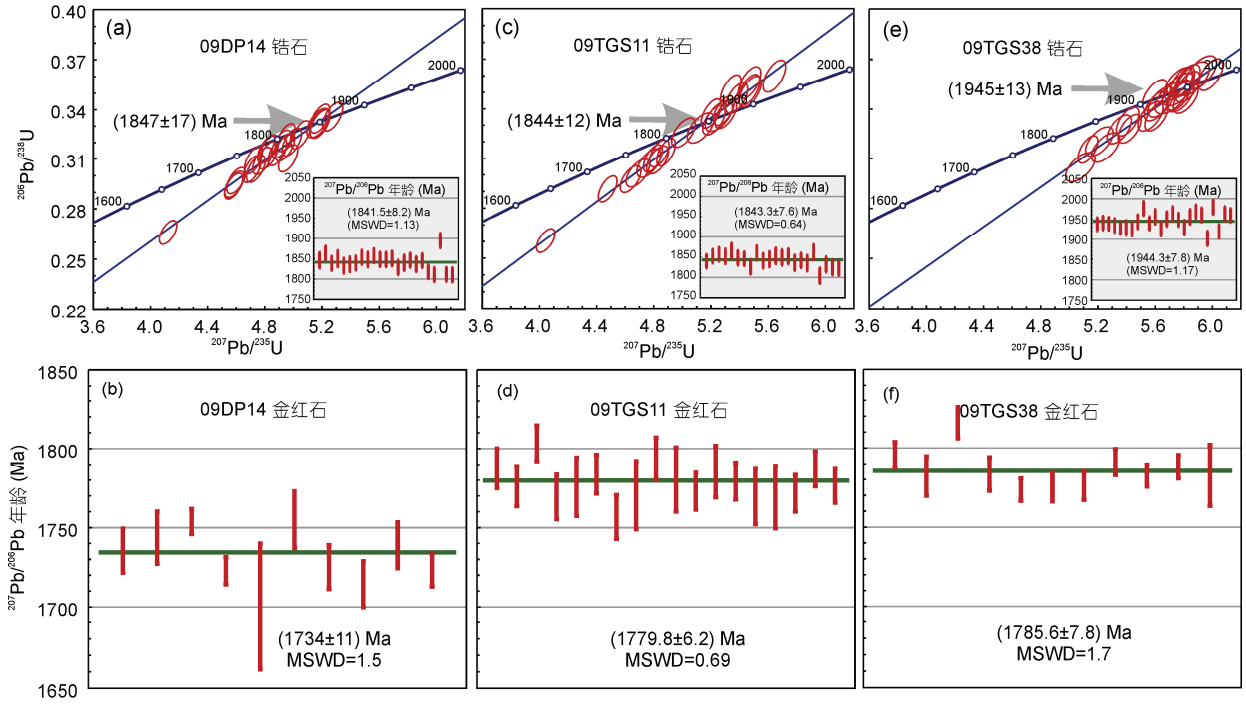

图 12　华北克拉通西部板块内部孔兹岩带的锆石和金红石的 U-Pb 年龄结果

Jiao等, 2011). 为验证金红石Hf同位素激光原位测定结果的可靠性, 对所有金红石样品均进行了溶液测定, 其结果与激光测定值一致, 表明本文的测试结果是可信的.

从总体情况来看, 该区金红石具有相对均一的Hf同位素组成(图13), 这与锆石的情况有所不同. 但是另一方面, 这些金红石又具有非常低的$^{176}Lu/^{177}Hf$比值, 明显低于锆石. 这表明金红石在Lu-Hf同位素体系封闭时, 富含重稀土的石榴石应该发生过大批量的结晶.

从不同地点来看, 大青山地区3件样品的金红石给出了几乎一致的Hf组成. 但尤以值得指出的是, 09DP14样品即夕线石榴片麻岩中金红石给出的Pb-Pb年龄为(1734±11)Ma. 该年龄明显低于锆石的U-Pb年龄(1841.5±8.2)Ma, 表明金红石的U-Pb体系封闭温度低于锆石. 如果将时间统一归并到1780Ma, 我们则发现锆石和金红石的Hf同位素组成在误差范围内并不重合.

对东部的集宁地区, 我们采集了4件样品以供研究. 同大青山地区类似, 4件样品金红石的Hf同位素组成也极为均匀, 但比值略高于大青山地区. 值得注意的是, 同样为夕线石榴片麻岩的09TGS11和09TGS38样品中的金红石给出一致的Pb-Pb年龄(~1780Ma), 但该2件样品的锆石却分别给出(1843.3±7.6)和(1944.3±7.8)Ma的Pb-Pb年龄. 09TGS38样品的锆石具有1.94 Ga的变质年龄, 且锆石和金红石具有几乎一致的Hf同位素组成, 表明金红石Hf同位素体系没有遭受后期变质事件的干扰, 其原始的Hf同位素特征被保留了下来. 而对于09TGS11样品, 其金红石的Hf同位素比值明显高于锆石, 因此我们推测金红石在结晶时具有不同于锆石的Hf元素来源.

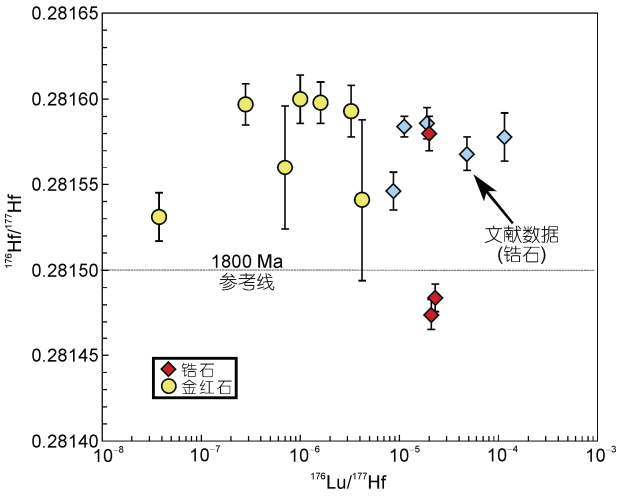

图 13　华北克拉通西部板块内部孔兹岩带的锆石和金红石 Lu-Hf 同位素组成

锆石(蓝色菱形)资料据 Santosh 等(2009)和 Yang 等(2014)

但如果将目前已发表的资料一并考虑(图13), 我们发现, 时间较老的1.92Ga左右超高温麻粒岩的锆石与金红石的Hf同位素组成基本一致, 而年龄相对年轻的麻粒岩中, 锆石与金红石的Hf同位素体系存在明显差别. 因此, 从Lu-Hf同位素体系来看, 华北克拉通西部孔兹岩带中的麻粒岩具有复杂的演化历史, 值得进一步深入研究.

6　结论

对目前金红石微区U-Pb定年标准物质JDX、R10、Sugluk-4和PCA-S207进行了$^{176}Hf/^{177}Hf$测定, 与溶液或文献报道值一致. 这表明, 对于低Hf含量(~50 ppm)的金红石, 采用我们建立的方法可以获得可靠的、有意义的$^{176}Hf/^{177}Hf$比值. 但测试过程中, 基体匹配的金红石参考标准必不可少, 也即锆石等其他矿物不能用来作为金红石Hf同位素激光原位测定的参考物质. 激光原位技术准确获得金红石Hf同位素的关键在于^{176}Hf的信号强度至少大于10mV, 因而需要较大的剥蚀束斑直径. 运用上述建立的方法, 本文对华北克拉通西部孔兹岩带不同地区麻粒岩中的金红石和锆石进行了Hf同位素测定, 结果表明这些麻粒岩经历过复杂的变质演化历史.

致谢　中国科学院地质与地球物理研究所李秋立研究员和英国地质调查局Laura Bracciali博士提供了金红石U-Pb年龄标准物质, 北京大学许成教授提供了Lu稀释剂, 审稿专家对文稿提出了很好的修改意见, 在此一并致以诚挚的谢意.

参考文献

董春艳, 万渝生, 徐仲元, 刘敦一, 杨振升, 马铭株, 颉颃强. 2012. 华北克拉通大青山地区古元古代晚期孔兹岩系: 锆石SHRIMP U-Pb定年. 中国科学: 地球科学, 42: 1851–1862

李秋立, 杨亚楠, 石永红, 林伟. 2013. 榴辉岩中金红石U-Pb定年: 对大陆碰撞造山带形成和演化的制约. 科学通报, 58: 2279–2284
卢良兆, 靳是琴, 徐学纯, 刘福来. 1992. 内蒙古东南部早前寒武纪孔兹岩系成因及其含矿性. 长春: 吉林科学技术出版社
卢良兆, 徐学纯, 刘福来. 1996. 中国北方早前寒武纪孔兹岩系. 长春: 长春出版社
谢烈文, 张艳斌, 张辉煌, 孙金凤, 吴福元. 2008. 斜锆石/锆石U-Pb和Lu-Hf同位素以及微量元素成分的同时原位测定. 科学通报, 53: 220–228
赵国春. 2009. 华北克拉通基底主要构造单元变质作用演化及其若干问题讨论. 岩石学报, 25: 1772–1792
赵国春, 孙敏, Wilde S A. 2002. 华北克拉通基底构造单元特征及早元古代拼合. 中国科学 D辑: 地球科学, 32: 538–549
Aulbach S, O'Reilly S Y, Griffin W L, Pearson N J. 2008. Subcontinental lithospheric mantle origin of high niobium/tantalum ratios in eclogites. Nat Geosci, 1: 468–472
Bracciali L, Parrish R R, Horstwood M S A, Condon D J, Najman Y. 2013. U-Pb LA-(MC)-ICP-MS dating of rutile: New reference materials and applications to sedimentary provenance. Chem Geol, 347: 82–101
Cherniak D J, Manchester J, Watson E B. 2007. Zr and Hf diffusion in rutile. Earth Planet Sci Lett, 261: 267–279
Choukroun M, O'Reilly S Y, Griffin W L, Pearson N J, Dawson J B. 2005. Hf isotopes of MARID (mica-amphibole-rutile-ilmenite-diopside) rutile trace metasomatic processes in the lithospheric mantle. Geology, 33: 45–48
Dan W, Li X H, Guo J H, Liu Y, Wang X C. 2012. Integrated *in situ* zircon U-Pb age and Hf-O isotopes for the Helanshan khondalites in North China Craton: Juvenile crustal materials deposited in active or passive continental margin? Precambrian Res, 222-223: 143–158
Ewing T A, Rubatto D, Eggins S M, Hermann J. 2011. *In situ* measurement of hafnium isotopes in rutile by LA-MC-ICPMS: Protocol and applications. Chem Geol, 281: 72–82
Ewing T A, Hermann J, Rubatto D. 2013. The robustness of the Zr-in-rutile and Ti-in-zircon thermometers during high-temperature metamorphism (Ivrea-Verbano Zone, northern Italy). Contrib Mineral Petrol, 165: 757–779
Ewing T A, Rubatto D, Hermann J. 2014. Hafnium isotopes and Zr/Hf of rutile and zircon from lower crustal metapelites (Ivrea-Verbano Zone, Italy): Implications for chemical differentiation of the crust. Earth Planet Sci Lett, 389: 106–118
Ferry J M, Watson E B. 2007. New thermodynamic models and revised calibrations for the Ti-in-zircon and Zr-in-rutile thermometers. Contrib Mineral Petrol, 154: 429–437
Guo J H, Peng P, Chen Y, Jiao S J, Windley B F. 2012. UHT sapphirine granulite metamorphism at 1.93–1.92 Ga caused by gabbronorite intrusions: Implications for tectonic evolution of the northern margin of the North China Craton. Precambrian Res, 222-223: 124–142
Hu Z C, Liu Y S, Gao S, Liu W G, Zhang W, Tong X R, Lin L, Zong K Q, Li M, Chen H H, Zhou L, Yang L. 2012. Improved *in situ* Hf isotope ratio analysis of zircon using newly designed X skimmer cone and jet sample cone in combination with the addition of nitrogen by laser ablation multiple collector ICP-MS. J Anal Atom Spectrom, 27: 1391–1399
Jiao S J, Guo J H. 2011. Application of the two-feldspar geothermometer to ultrahigh-temperature (UHT) rocks in the Khondalite belt, North China craton and its implications. Am Mineral, 96: 250–260
Jiao S J, Guo J H, Mao Q, Zhao R F. 2011. Application of Zr-in-rutile thermometry: A case study from ultrahigh-temperature granulites of the Khondalite belt, North China Craton. Contrib Mineral Petrol, 162: 379–393
Jiao S J, Guo J H, Harley S L, Peng P. 2013. Geochronology and trace element geochemistry of zircon, monazite and garnet from the garnetite and/or associated other high-grade rocks: Implications for Palaeoproterozoic tectonothermal evolution of the Khondalite Belt, North China Craton. Precambrian Res, 237: 78–100
Li Q L, Lin W, Su W, Li X H, Shi Y H, Liu Y, Tang G Q. 2011a. SIMS U-Pb rutile age of low-temperature eclogites from southwestern Chinese Tianshan, NW China. Lithos, 122: 76–86
Li X P, Yang Z Y, Zhao G C, Grapes R, Guo J H. 2011b. Geochronology of khondalite-series rocks of the Jining Complex: Confirmation of depositional age and tectonometamorphic evolution of the North China Craton. Int Geol Rev, 53: 1194–1211
Liu S J, Dong C Y, Xu Z Y, Santosh M, Ma M Z, Xie H Q, Liu D Y, Wan Y S. 2013. Palaeoproterozoic episodic magmatism and high-grade metamorphism in the North China Craton: Evidence from SHRIMP zircon dating of magmatic suites in the Daqingshan area. Geol J, 48: 429–455
Luvizotto G L, Zack T, Meyer H P, Ludwig T, Triebold S, Kronz A, Münker C, Stockli D F, Prowatke S, Klemme S, Jacob D E, von Eynatten H. 2009. Rutile crystals as potential trace element and isotope mineral standards for microanalysis. Chem Geol, 261: 346–369
Ma M Z, Wan Y S, Santosh M, Xu Z Y, Xie H Q, Dong C Y, Liu D Y, Guo C L. 2012. Decoding multiple tectonothermal events in zircons from single rock samples: SHRIMP zircon U-Pb data from the late Neoarchean rocks of Daqingshan, North China Craton. Gondwana Res, 22: 810–827
Meinhold G. 2010. Rutile and its applications in earth sciences. Earth-Sci Rev, 102: 1–28
Morisset C E, Scoates J S, Weis D, Rahier A. 2014. Methodology and application of hafnium isotopes in ilmenite and rutile by MC-ICP-MS. Geostand Geoanal Res, 38: 159–176
Nowell G M, Kempton P D, Noble S R, Fitton J G, Saunders A D, Mahoney J J, Taylor R N. 1998. High precision Hf isotope measurements of MORB and OIB by thermal ionization mass spectrometry: Insight into the depleted mantle. Chem Geol, 149: 211–233
Peng P, Wang X P, Windley B F, Guo J H, Zhai M G, Li Y. 2014.

Spatial distribution of ~1950–1800 Ma metamorphic events in the North China Craton: Implications for tectonic subdivision of the craton. Lithos, 202-203: 250–266

Santosh M, Wilde S A, Li J H. 2007. Timing of Paleoproterozoic ultrahigh-temperature metamorphism in the North China Craton: Evidence from SHRIMP U-Pb zircon geochronology. Precambrian Res, 159: 178–196

Santosh M, Wan Y S, Liu D Y, Dong C Y, Li J H. 2009. Anatomy of Zircons from an ultrahot orogen: The amalgamation of the North China Craton within the Supercontinent Columbia. J Geol, 117: 429–443

Thirlwall M F, Walder A J. 1995. *In situ* hafnium isotope ratio analysis of zircon by inductively coupled plasma multiple collector mass spectrometry. Chem Geol, 122: 241–247

Thirlwall M F, Anczkiewicz R. 2004. Multidynamic isotope ratio analysis using MC-ICP-MS and the causes of secular drift in Hf, Nd and Pb isotope ratios. Int J Mass Spectrom, 235: 59–81

Tomkins H S, Powell R, Ellis D J. 2007. The pressure dependence of the zirconium-in-rutile thermometer. J Metamorph Geol, 25: 703–713

Vry J K, Baker J A. 2006. LA-MC-ICPMS Pb-Pb dating of rutile from slowly cooled granulites: Confirmation of the high closure temperature for Pb diffusion in rutile. Geochim Cosmochim Acta, 70: 1807–1820

Wan Y S, Song B, Liu D Y, Wilde S A, Wu J S, Shi Y R, Yin X Y, Zhou H Y. 2006. SHRIMP U-Pb zircon geochronology of Palaeoproterozoic metasedimentary rocks in the North China Craton: Evidence for a major Late Palaeoproterozoic tectonothermal event. Precambrian Res, 149: 249–271

Wan Y S, Liu D Y, Dong C Y, Xu Z Y, Wang Z J, Wilde S A, Liu Z H, Yang Z S, Zhou H Y. 2009. The Precambrian Khondalite Belt in the Daqingshan area, North China Craton: Evidence for multiple metamorphic events in the Palaeoproterozoic era. Geol Soc Spec Publ, 323: 73–97

Watson E B, Wark D A, Thomas J B. 2006. Crystallization thermometers for zircon and rutile. Contrib Mineral Petrol, 151: 413–433

Wu F Y, Yang Y H, Xie L W, Yang J H, Xu P. 2006. Hf isotopic compositions of the standard zircons and baddeleyites used in U-Pb geochronology. Chem Geol, 234: 105–126

Xia X P, Sun M, Zhao G C, Luo Y. 2006. LA-ICP-MS U-Pb geochronology of detrital zircons from the Jining Complex, North China Craton and its tectonic significance. Precambrian Res, 144: 199–212

Xia X P, Sun M, Zhao G C, Wu F Y, Xu P, Zhang J, He Y H. 2008. Paleoproterozoic crustal growth in the Western Block of the North China Craton: Evidence from detrital zircon Hf and whole rock Sr-Nd isotopic compositions of the Khondalites from the Jining Complex. Am J Sci, 308: 304–327

Yang Q Y, Santosh M, Tsunogae T. 2014. Ultrahigh-temperature metamorphism under isobaric heating: New evidence from the North China Craton. J Asian Earth Sci, 95: 2–16

Yang Y H, Zhang H F, Chu Z Y, Xie L W, Wu F Y. 2010. Combined chemical separation of Lu, Hf, Rb, Sr, Sm and Nd from a single rock digest and precise and accurate isotope determinations of Lu-Hf, Rb-Sr, and Sm-Nd isotope systems using Multi-Collector ICP-MS and TIMS. Int J Mass Spectrom, 290: 120–126

Yin C Q, Zhao G C, Sun M, Xia X P, Wei C J, Zhou X W, Leung W. 2009. LA-ICP-MS U-Pb zircon ages of the Qianlishan Complex: Constrains on the evolution of the Khondalite Belt in the Western Block of the North China Craton. Precambrian Res, 174: 78–94

Yin C Q, Zhao G C, Guo J H, Sun M, Xia X P, Zhou X W, Liu C H. 2011. U-Pb and Hf isotopic study of zircons of the Helanshan Complex: Constrains on the evolution of the Khondalite Belt in the Western Block of the North China Craton. Lithos, 122: 25–38

Yuan H L, Gao S, Dai M N, Zong C L, Günther D, Fontaine G H, Liu X M, Diwu C R. 2008. Simultaneous determinations of U-Pb age, Hf isotopes and trace element compositions of zircon by excimer laser-ablation quadrupole and multiple-collector ICP-MS. Chem Geol, 247: 100–118

Zack T, Kronz A, Foley S F, Rivers T. 2002. Trace element abundances in rutiles from eclogites and associated garnet mica schists. Chem Geol, 184: 97–122

Zack T, Moraes R, Kronz A. 2004a. Temperature dependence of Zr in rutile: empirical calibration of a rutile thermometer. Contrib Mineral Petrol, 148: 471–488

Zack T, von Eynatten H, Kronz A. 2004b. Rutile geochemistry and its potential use in quantitative provenance studies. Sediment Geol, 171: 37–58

Zhao G C, Wilde S A, Cawood P A, Lu L Z. 1999. Tectonothermal history of the basement rocks in the western zone of the North China Craton and its tectonic implications. Tectonophysics, 310: 37–53

Zhao G C, Sun M, Wilde S A, Li S Z. 2005. Late Archean to Paleoproterozoic evolution of the North China Craton: Key issues revisited. Precambrian Res, 136: 177–202

Zhao G C, Wilde S A, Guo J H, Cawood P A, Sun M, Li X P. 2010. Single zircon grains record two Paleoproterozoic collisional events in the North China Craton. Precambrian Res, 177: 266–276

Zhao G C, Cawood P A, Li S Z, Wilde S A, Sun M, Zhang J, He Y H, Yin C Q. 2012. Amalgamation of the North China Craton: Key issues and discussion. Precambrian Res, 222-223: 55–76

SCIENCE CHINA
Earth Sciences

• RESEARCH PAPER •

December 2015 Vol.58 No.12: 2134–2144
doi: 10.1007/s11430-015-5215-2

In situ determination of hafnium isotopes from rutile using LA-MC-ICP-MS

LI Yang[1,2], YANG YueHeng[1*], JIAO ShuJuan[1], WU FuYuan[1], YANG JinHui[1], XIE LieWen[1] & HUANG Chao[1]

[1] *State Key Laboratory of Lithospheric Evolution, Institute of Geology and Geophysics, Chinese Academy of Sciences, Beijing 100029, China;*
[2] *College of Earth Science, University of Chinese Academy of Sciences, Beijing 100049, China*

Received May 5, 2015; accepted August 20, 2015; published online November 11, 2015

The hafnium isotopic analysis using laser ablation has been widely conducted on Hf-rich minerals (zircon/baddeleyite/calzirtite/eudialyte), however, little work has been reported on Hf-poor (<100 ppm) minerals. This work presents a detailed procedure of *in situ* hafnium isotopic analysis from rutile using laser ablation multiple collector inductively coupled plasma mass spectrometry (LA-MC-ICP-MS). The rutile U-Pb dating reference material JDX shows homogeneous hafnium isotopic ratios, with $^{176}Hf/^{177}Hf$=0.281795±0.000015 (2SD, n=33) and $^{176}Lu/^{177}Hf$=0.000018±0.000004 (2SD, n=17) that suggest the possibility of using JDX as a new reference material hafnium isotopic measurement. We also measure hafnium isotopic compositions of other rutile U-Pb dating reference material (R10, Sugluk-4 and PCA-S207) and the $^{176}Hf/^{177}Hf$ values are similar to previously reported results, which confirms that we can acquire accurate and precise hafnium isotopic compositions using our developed analytical protocol. We analyzed hafnium isotopic compositions and U-Pb ages of rutile in high-temperature and ultrahigh-temperature granulites from various terrains of the Khondalite Belt from the North China Craton, combined with zircon results in the same area, suggesting that the metamorphic evolution history of the granulite is much more complicated than previously thought.

rutile, hafnium isotope, *in situ* laser ablation, MC-ICP-MS, khondalite

Citation: Li Y, Yang Y H, Jiao S J, Wu F Y, Yang J H, Xie L W, Huang C. 2015. *In situ* determination of hafnium isotopes from rutile using LA-MC-ICP-MS. Science China: Earth Sciences, 58: 2134−2144, doi: 10.1007/s11430-015-5215-2

Rutile is an accessory mineral and widely distributed in magmatic, metamorphic and sedimentary rocks. The formation of rutile, particularly in mafic metamorphic rocks, is usually associated with metamorphic reactions and it is considered as an indicator mineral of greenschist, eclogite and granulite facies (Meinhold, 2010). Rutile contains sufficient uranium to allow an attractive *in situ* U-Pb dating for geochronology research (Vry and Baker, 2006; Li et al., 2011, 2013; Bracciali et al., 2013). Furthermore, rutile is a major host mineral for Nb, Ta and other high field strength element and its trace element geochemistry gives significant amounts of provenance information (Zack et al., 2002, 2004b; Luvizotto et al., 2009). Additionally, the recent studies show that the Zr incorporation in rutile is strongly temperature and pressure dependent and the Zr-in-rutile thermometry can provide interesting information of geological evolution history (Zack et al., 2004a; Watson et al., 2006; Cherniak et al., 2007; Ferry and Watson, 2007; Tomkins et al., 2007; Ewing et al., 2013). Consequently, researchers have been exploring *in situ* Hf isotope analysis in rutile for establishing similar (to zircon) research system of tracing geological evolution history, which consists of U-Pb age, trace element, temperature condition and hafnium iso-

*Corresponding author (email: yangyueheng@mail.iggcas.ac.cn)

topic characteristic (Choukroun et al., 2005; Morisset et al., 2014). These important features of zircon and rutile can therefore provide complementary provenance information for samples with complex history (Ewing et al., 2014).

However, compared with zircon, *in situ* Hf isotope determination from rutile using laser ablation is quite challenging. The first problem is the lack of matrix-matched Hf isotope analysis standards, in other words, it is still unknown whether zircon or other minerals can be used as external standards for *in situ* Hf isotope measurement of rutile; the second problem is the Hf content of rutile is very low (usually <50 ppm), which results in low signal intensity and impacts on analytical precision. Besides, rutile also contains extremely low Yb and Lu content. This characteristic hinders for acquiring accurate mass bias coefficient for Yb and Lu, nevertheless, it also suggests dispensability of interference correction for Yb and Lu, and we need to figure out the Hf isotope uncertainty caused by them. Despite many researchers' explorations and attempts, a number of critical issues remain to be solved (Choukroun et al., 2005; Aulbach et al., 2008; Ewing et al., 2011).

It is under this situation that we establish the analytical procedure of *in situ* rutile Hf isotope analysis using Neptune MC-ICP-MS connected with a 193 nm laser transmitter. Based on in-house rutile standards developed by us, we measure *in situ* Hf isotope ratios of rutile U-Pb dating reference materials, which are in agreement with solution results by isotopic dilution method. We also analyze Hf isotopes of rutile from khondalites in the western block of the North China Craton, as well as their trace element and U-Pb ages, and propose that the evolution history of the Khondalite Belt is much more complicated than previously thought, demonstrating the prospect of its application in geology.

1 Introduction of U-Pb dating reference rutile

In this study, we analyze Hf isotopic composition of rutile U-Pb dating reference materials. JDX rutile is a single large euhedral crystal about 5 cm in length, 5 cm in width and 2.5 cm in thickness with its unclear origin. It is used as U-Pb dating monitoring standard in secondary ion mass spectrometer laboratory at Institute of Geology and Geophysics of Chinese Academy of Science and its $^{206}Pb/^{238}U$ weighted average age is 509±8 Ma (Li et al., 2011) (Figure 1(a)). R10 rutile used in this study is a piece of fragment of a large single crystal from Gjerstad, south Norway (Luvizotto et al., 2009; Figure 1(b)). Sugluk-4 rutile (100 to 500 μm) is collected from a granulite facies quartzite in the Ungava segment of the Trans-Hudson orogen of Canada. The grains are translucent, brown-red and idioblastic to sub-idioblastic (Bracciali et al., 2013; Figure 1(c)). PCA-S207 rutile is collected from a highly strained granulite facies paragneiss of the East Lake Athabasca region, Canada. The grains are commonly xenoblastic and range in size from a few tens of micron to several hundreds of micron, and its color is red-brown to dark brown (Bracciali et al., 2013; Figure 1(d)). The trace element compositions of rutiles are listed in Table 1 and their Hf contents are all below 50 ppm, and both Yb and Lu contents are extremely low. Except for R10, other reference rutiles' hafnium isotopes have not been reported yet (Luvizotto et al., 2009).

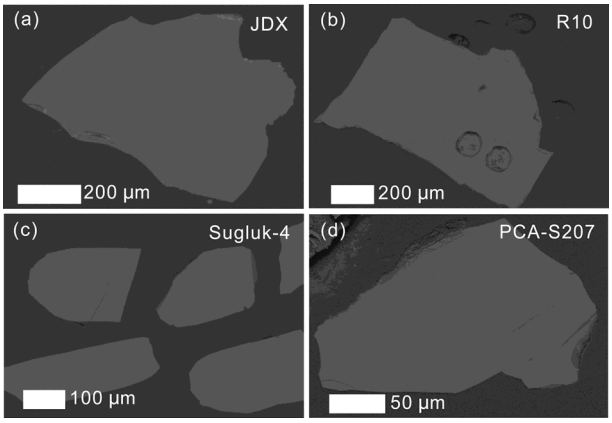

Figure 1 Back Scattered Electron images of rutile reference materials.

2 Analytical procedure

In situ Hf isotope analysis was carried out at the Institute of Geology and Geophysics of Chinese Academy of Sciences using GeoLas Pro 193 nm excimer laser ablation system coupled to Thermo Finnigan Neptune MC-ICP-MS, and introduction of these instruments can be found in Wu et al. (2006) and Xie et al. (2008).

The sample preparation for rutile Hf isotope analysis is similar to that of zircon (Wu et al., 2006; Xie et al., 2008): handpicked rutile grains are mounted in epoxy resin and polished until the grain centers are well exposed. Before analysis, the target is rinsed with 2% dilute nitric acid and wiped with ethanol to remove any potential contamination.

Table 1 Trace element compositions of U-Pb dating reference rutile (unit: ppm)

Element	JDX[a)]	R10[b)]	Sugluk-4[c)]	PCA-S207[c)]
Zr	308	778	836	977
Nb	337	2659	1461	1265
Yb	0.015			
Lu	0.0064	0.041		
Hf	50	38	51	37
Ta	64	480	105	46
W		108	221	18
Pb	0.52	0.081	16	8
Th	0.005	<0.004		
U	1.1	44.1	59.5	22.8

a) This study; b) Luvizotto et al. (2009); c) Bracciali et al. (2013).

The procedure of *in situ* Hf isotope measurement for rutile is analogous to that of zircon (or baddeleyite) (Wu et al., 2006; Xie et al., 2008). The typical operating parameters and Faraday cup configurations are listed in Table 2. Rutile is analyzed with spot diameter of 60, 90, 120 and 160 μm, and the ablated material is introduced into Neptune MC-ICP-MS by Helium gas.

2.1 Solution analysis

The solution method for rutile Hf isotope includes sample digestion, chemical purification and mass spectrometry measurement. Approximately 50 mg rutile power is added into 10 mL bomb, together with separate ^{180}Hf and ^{176}Lu spikes and mixed with concentrated acid HF-HNO_3-$HClO_4$ (2 mL-1 mL-0.1 mL). Then the bomb is heated in bake oven at 190°C for a week till complete digestion and sample-spike equilibration. After cooling, the bomb is opened and evaporated to fume HF at 130°C and increase the temperature to 180°C to evaporate $HClO_4$ to complete dryness. Finally, the residue is dissolved in 5 mL of 3 mol/L HCl for the second bomb digestion at a temperature of 100°C for 12 h prior to chemical purification. The Lu-Hf purification is performed by Ln Spec resin. At the first stage, the matrix elements (including Light and Middle Rare Earth Element) are eluted with 3 mol/L HCl. The Lu (+Yb) fraction is then eluted and collected with 4 mol/L HCl, evaporated to dryness and ready for mass spectrometry. To minimize the isobaric interference of ^{176}Lu and ^{176}Yb on ^{176}Hf, the column is rinsed with 6 mol/L HCl to remove Lu/Yb residue before collecting Hf fraction. Then Ti is separated from Hf using 4 mol/L HCl+0.5% H_2O_2. At the second stage, the Hf fraction is extracted from the column with 5 mL of 2 mol/L HF and gently evaporated to dryness. Finally, this fraction is taken up into a centrifuge tube with 0.8 mL 2% HNO_3 and ready for Hf isotope analysis. More details of chemical purification and mass spectrometry measurement can be found in Yang et al. (2010).

Before mass spectrometry analysis, the Neptune MC-ICP-MS is tuned for sensitivity and peak shape using 200 ppb AlfaHf standard solution. The accuracy and reproducibility of analytical results are examined using 50 ppb JMC475 standard solution as shown in Figure 2 that fifteen analyses of JMC475 give a weighted mean ^{176}Hf/^{177}Hf of 0.282172±0.000029 (2SD, n=15), which is in good agreement with the value determined by Nowell et al. (1998).

2.2 *In situ* laser ablation analysis

2.2.1 *JDX rutile Hf isotope evaluation*

Although several rutile U-Pb reference materials for *in situ* geochronology have been reported (Luvizotto et al., 2009; Li et al., 2011; Bracciali et al., 2013), there is still scarcity of rutile Hf isotope reference material. Except for R10, other rutiles' Hf isotope composition has not been reported yet (Luvizotto et al., 2009).

Firstly, using isotopic dilution method, we analyze the

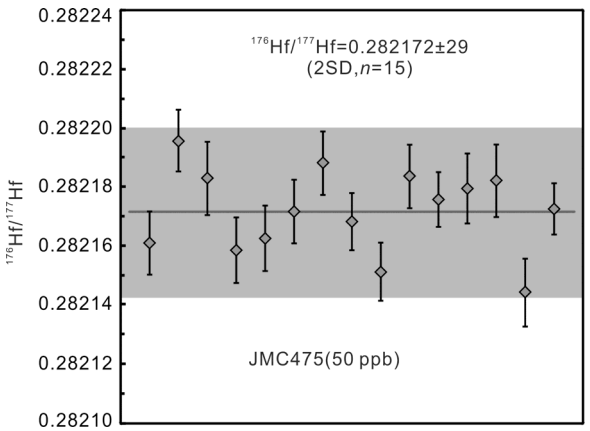

Figure 2 50 ppb JMC475 Hf standard solution for monitoring stability of MC-ICP-MS. The grey area represents weighted average value.

Table 2 Typical operating parameters and Faraday cup configuration

Neptune MC-ICP-MS					Laser ablation system			
RF forward power			1250 W		Instrument model		Geolas Pro	
Cooling gas			16 L/min		Wave length		UV 193 nm	
Auxiliary gas			0.8 L/min		Energy density		12 J/cm^2	
Extraction			–2000 V		Spot diameter (μm)		60, 90, 120, 160	
Focus			–645 V		Laser frequency		20 Hz	
Instrument resolution			~400		Carrier gas flow		0.83 L/min	
Sampling mode (solution)			9 blocks of 10 cycles					
Sampling mode (laser)			1 block of 200 cycles					
Integration time			4.194 s (solution) or 0.262 s (laser)					
Faraday cup configuration								
Faraday cup	L4	L3	L2	L1	Center	H1	H2	H3
Nominal mass	172	173	175	176	177	178	179	180
Hf				Hf	Hf	Hf	Hf	Hf
Yb/Lu	Yb	Yb	Lu	Yb+Lu				

Lu and Hf contents, and Lu-Hf isotopic composition of 12 chips of JDX rutile grains for multiple times in different periods as shown in Figure 3. The Hf content of JDX is 50.1±0.7 ppm (2SD, n=17), Lu content is 0.0064±0.0014 ppm (2SD, n=17), $^{176}Lu/^{177}Hf$= 0.000018±0.000004 (2SD, n=17), $^{176}Hf/^{177}Hf$=0.281795±0.000015 (2SD, n=33).

After the Hf isotopic composition of JDX rutile is confirmed by isotope dilution, the JDX rutile is tested by *in situ* laser ablation method over a long period of time as shown in Figure 4. The $^{176}Hf/^{177}Hf$ and $^{177}Hf/^{179}Hf$ values fall into quite narrow ranges (fractional correction is not carried out), indicating that JDX rutile is suitable to serve as in-house Hf isotope standards. Li et al. (2011) determined U-Pb system of JDX rutile and found JDX is slight disconcordant, thus JDX rutile usually serves as monitoring standards. However, our study shows that JDX contains sufficient Hf and coincident $^{176}Hf/^{177}Hf$ value. Therefore, it can serve as in-house standard material for *in situ* Hf isotope analysis of rutile by LA-MC-ICP-MS.

2.2.2 *Isobaric interference correction*

Isobaric interferences on ^{176}Hf usually arise from ^{176}Yb and ^{176}Lu, and are often corrected by monitoring interference-free ^{173}Yb and ^{175}Lu (Thirlwall and Walder, 1995; Thirlwall and Anczkiewicz, 2004; Wu et al., 2006; Yuan et al., 2008; Hu et al., 2012). As mentioned above, on the one hand, due to the low Yb and Lu contents in rutile, there exists possibility of neglecting Yb and Lu interferences during analysis; on the other hand, given the relatively low Hf content in rutile, although rutile contains little Yb or Lu, it requires correction for their contribution to mass 176. Consequently, it is necessary to compare their differences and evaluate the influence of low Yb and Lu contents on Hf isotope measurement in rutile.

If Yb and Lu interference correction is applied, its principle is similar to that of zircon:

$$^{176}Hf=^{176}M-[^{175}Lu_m\times(^{176}Lu/^{175}Lu)_t(M_{176}/M_{175})^{\beta Yb}+ {}^{172}Yb_m\times(^{176}Yb/^{172}Yb)_t(M_{176}/M_{172})^{\beta Yb}]. \quad (1)$$

Mass bias is corrected using an exponential law and the mass bias coefficient for Hf (β_{Hf}) is calculated using $^{179}Hf/^{177}Hf$=0.7325. For zircon, the Yb mass bias coefficient β_{Yb} is calculated from measured ^{172}Yb and ^{173}Yb using $^{172}Yb/^{173}Yb$=1.35272. It is not possible to independently calculate the mass bias coefficient for Lu, thus β_{Yb} is used to substitute it. For rutile analysis, it is impossible to determine β_{Yb} due to very low Yb content, hence β_{Hf} is used to correct Yb and Lu.

If Yb and Lu interference correction is not applied, the entire signal intensity received by 176 mass Faraday cup is ^{176}Hf. We measure $^{176}Hf/^{177}Hf$ ratio of JDX and R10 rutile for fifteen times respectively and compare the results (Figure 5). For JDX, if Yb and Lu interference correction is not applied, $^{176}Hf/^{177}Hf$=0.28204±0.00019 (2SD), if applied, $^{176}Hf/^{177}Hf$=0.28180±0.00013 (2SD); For R10, if Yb and Lu interference correction is not applied, $^{176}Hf/^{177}Hf$= 0.28262±0.00057 (2SD), if applied, $^{176}Hf/^{177}Hf$=0.28219± 0.00016 (2SD). Obviously, application of Yb and Lu interference correction can notably improve accuracy and precision of $^{176}Hf/^{177}Hf$ value of rutile, and further evidence can be seen in Figure 6. In this study we analyzed four rutile reference material and two zircon standards (Mud Tank and GJ-1). In general Yb and Lu contents of rutile are very low, however there is some variation in Lu and Yb contents between different rutile minerals, and some rutile may contain Yb and Lu contents commensurate with those of zircon, suggesting the necessity of interference correction of Yb and Lu. Therefore, we applied interference correction in later Hf isotope analysis.

2.2.3 *Matrix effect*

In contrast to solution Hf isotope analysis, a matrix-matched standard mineral is needed for Hf isotope determination by

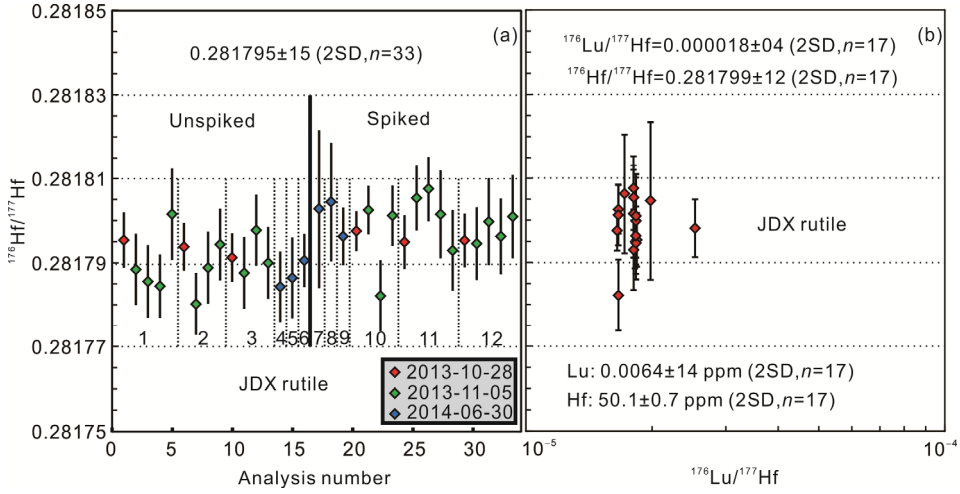

Figure 3 The Lu-Hf isotope analytical results of JDX rutile by isotopic dilution method in different periods. (a) $^{176}Hf/^{177}Hf$ ratio in 1 to 6 unspiked samples and in 7 to 12 spiked samples; (b) $^{176}Lu/^{177}Hf$ vs $^{176}Hf/^{177}Hf$ isotopic systematics.

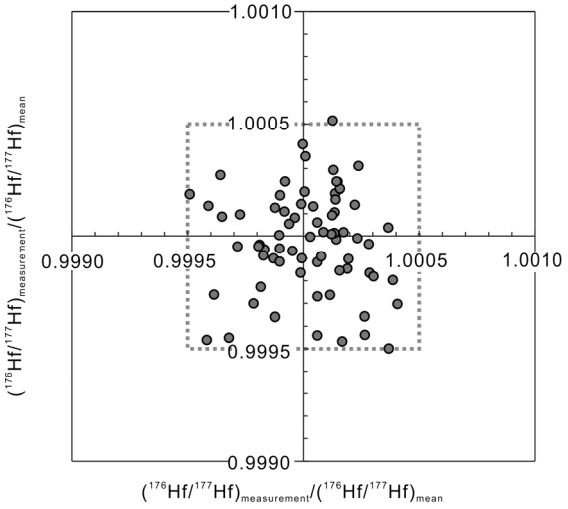

Figure 4 Homogeneity examination of Hf isotopic composition in JDX rutile.

in situ laser ablation. Compared with well-established Hf isotope analysis in zircon, *in situ* Hf isotope measurement in rutile is very challenging. One reason is the lack of matrix-matched Hf isotope standards, or rather it is still doubtful whether zircon (91500, Mud Tank or GJ-1) can be used as external standards for *in situ* Hf isotope measurement of rutile (Choukroun et al., 2005; Ewing et al., 2011).

To solve the problem, using zircon Mud Tank as standard, we analyze Hf isotope ratios of zircon and rutile using the same instrumental parameters. As shown in Figure 7, although the $^{176}Hf/^{177}Hf$ value of zircon GJ-1 is accurate (Figure 7(a)), there is significant systematic deviation between laser ablation results and solution results of JDX rutile (Figure 7(b)), which means zircon cannot be used as standard material for *in situ* Hf isotope analysis of rutile. This might be due to the following reasons: the first reason is the difference in chemical composition between zircon and rutile that lead to different fractionation behavior during laser ablation and mass spectrometry analysis; the second reason is the large difference of Hf contents between zircon (thousands of parts per million) and rutile (tens of parts per million) that makes it difficult to analyze Hf isotope of zir-

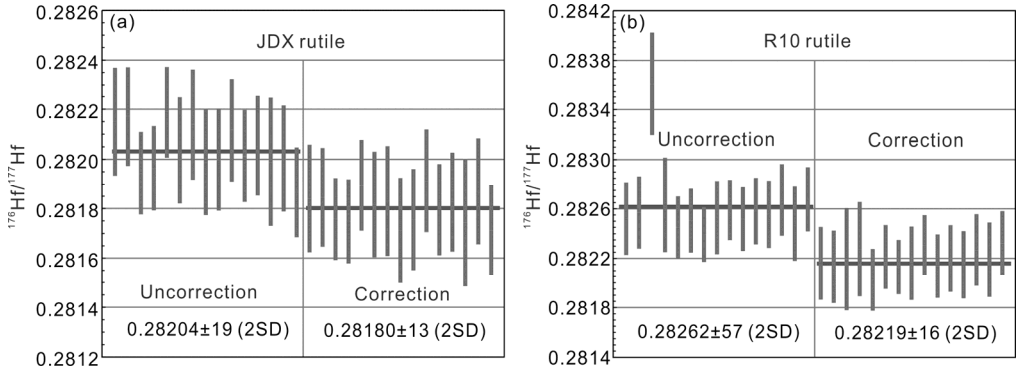

Figure 5 Comparison of *in situ* $^{176}Hf/^{177}Hf$ isotopic analysis between application of isobaric corrected and uncorrected Yb-Lu from JDX and R10 rutiles.

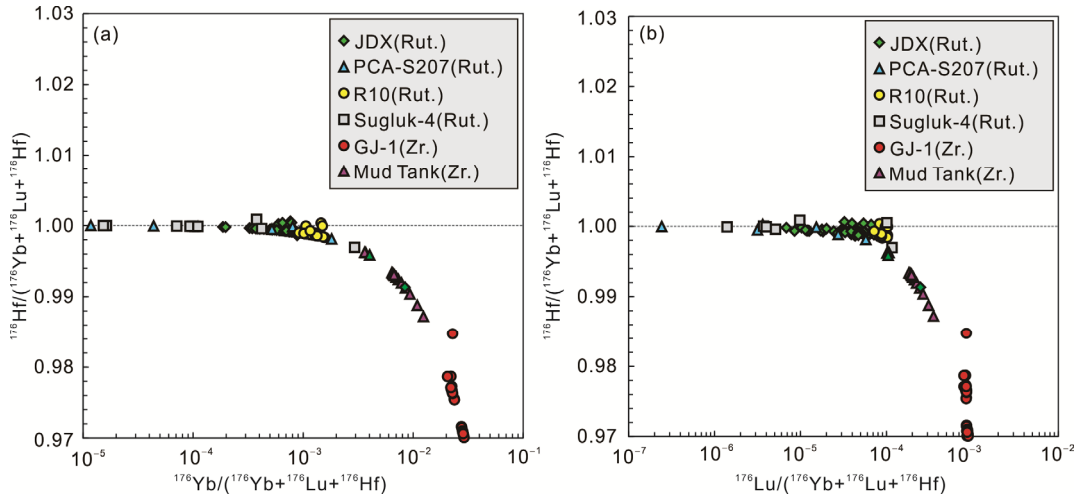

Figure 6 Signal intensity of mass 176 of reference rutile (JDX, R10, PCA-S207 and Sugluk-4) and standard zircon (Mud Tank and GJ-1). The main isobaric interference of ^{176}Hf is ^{176}Yb, and several rutile grains contain ^{176}Yb interference commensurate with those of standard zircon Mud Tank, suggesting the necessity of interference correction of Yb and Lu.

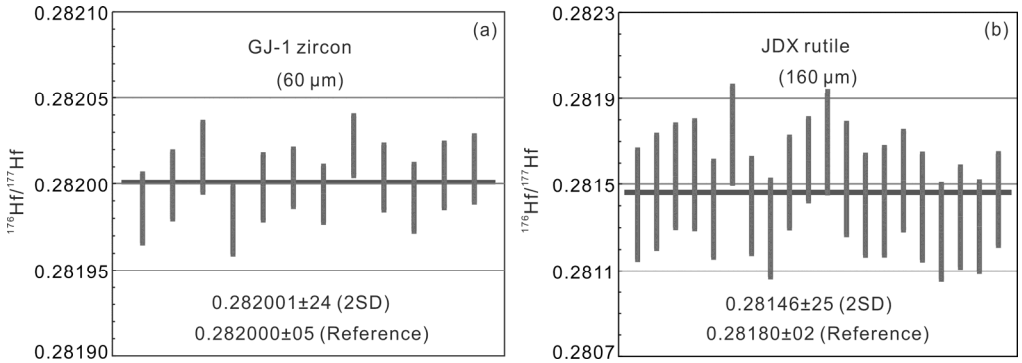

Figure 7 The matrix effect in Hf isotope analysis of zircon and rutile.

con and rutile with the same laser parameter. Consequently, we use JDX rutile as standard in later Hf isotope analysis of rutile.

3 Results and discussions

3.1 Hf isotopic composition of rutile U-Pb reference material

R10 rutile is a large single crystal from Gjerstad, south Norway, its Hf content is 37.4±0.4 ppm (rim) and 38.9±0.4 ppm (core), and Lu content is 0.0513±0.0005 ppm (rim) and 0.0300±0.0100 ppm (core). The $^{176}Hf/^{177}Hf$ ratios are 0.282178±0.000009 (rim) and 0.282178±0.000012 (core) (Luvizotto et al., 2009). The R10 rutile used in this study is a piece of fragment with 1.5 mm in length and 0.5 mm in width (Figure 1(b)). Using spots with a diameter of 160 μm, 42 LA-MC-ICP-MS analyses give reproducible $^{176}Hf/^{177}Hf$ values with a weighted mean of 0.282157±0.000204 (2SD, *n*=42), which is in a good agreement with the value determined by ID-MC-ICP-MS (Figure 8)(Luvizotto et al., 2009). With a 233 μm spot employed, Ewing et al. (2011) give a weighted mean of 0.282199±0.000280 (2SD, *n*=3).

Sugluk-4 rutile comes from a granulite facies quartzite in the Ungava segment of the Trans-Hudson orogen of Canada, which falls in a grain size range of 100 to 500 μm. The grains are translucent, brown-red and idioblastic to subidioblastic, with an average Hf content of 51 ppm (ranging from 36 to 67 ppm). PCA-S207 rutile is collected from a highly strained granulite facies paragneiss of the East Lake Athabasca region (Canada). The grains are commonly xenoblastic and range in size from a few tens of micron to several hundreds of micron, and its colours are red-brown to dark brown, with an average Hf content of 37 ppm (ranging from 20 to 60 ppm). Their LA-MC-ICP-MS U-Pb age is 1719±14 and 1865±7.5 Ma respectively (Bracciali et al., 2013), however their Hf isotopes have not been reported. Using spots with a diameter of 160 μm, 15 LA-MC-ICP-MS analyses of Sugluk-4 and PCA-S207 give a weighted mean $^{176}Hf/^{177}Hf$ of 0.281172±0.000107 (2SD) and 0.281246±0.000146 (2SD), respectively (Table 3, Figure 8).

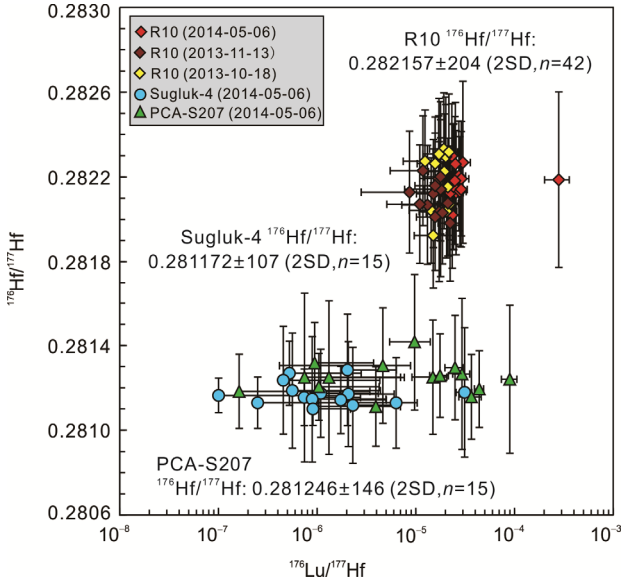

Figure 8 Lu-Hf isotopic compositions of rutile reference materials (R10, Sugluk-4 and PCA-S207) by LA-MC-ICP-MS.

According to the U-Pb isotopic system of R10, Sugluk-4 and PCA-S207, Bracciali et al. (2013) points out that R10 has a large degree of intergrain heterogeneity with respect to common Pb, nevertheless, Sugluk-4 and PCA-S207 appear to be suitable for primary and secondary reference materials of rutile U-Pb dating by LA-ICP-MS without the requirement for correction of common Pb (the reproducibility of $^{207}Pb/^{206}Pb$ and $^{206}Pb/^{238}U$ in Sugluk-4 is slightly better than that in PCA-S207). Sugluk-4 rutile show higher Hf contents and more homogeneous $^{176}Hf/^{177}Hf$ values than PCA-S207, making it better Hf isotope analysis standard. Consequently, it is possible for Sugluk-4 rutile to be used for both U-Pb dating and Hf isotope analysis standard simultaneously. However, more work is needed to verify the conclusion above due to limited rutile grains and isotopic data in this study.

3.2 Obtaining accurate Hf isotopic composition of rutile by laser ablation method

Owing to low Hf content (~50 ppm) in rutile, the Hf signal is very weak during laser ablation and sampling. It is not still yet reported what the exact lower limit of signal intensity for acquiring accurate Hf isotopic ratio is. To address this issue, we use solution sampling to simulate laser ablation sampling, using JMC475 standard solution with different concentration (50, 25, 10, 5, 2.5 and 1 ppb), and the results are shown in Figure 9(b). The Hf signal intensity declines as solution concentration decreases; when the ^{176}Hf signal reduces to ~10 mV, the ^{176}Hf/^{177}Hf values deviate notably from its true value. It may be caused by the weak signal intensity: the signal is so low that it nearly reaches detection limit of MC-ICP-MS, and this is also supported by our laser ablation data (Figure 9(a)). Given all that, we propose that, to acquire reliable ^{176}Hf/^{177}Hf values, the ^{176}Hf signal should be above 10 mV during *in situ* rutile Hf isotope analysis by LA-MC-ICP-MS. In practical analysis, the signal intensity can be controlled by choosing different spot sizes.

The appropriate hafnium content in rutile for accurate Hf isotope analysis has been illustrated in Figure 10. According to Hf isotopic data by LA-MC-ICP-MS shown above, the more hafnium rutile contains or the larger spot diameter we choose, the stronger signal intensity we have, thus the better precision we acquire. If assume the error of practical geological application is $\pm 3.5\varepsilon$ unit, the corresponding ^{176}Hf/^{177}Hf error is 0.0001. With a spot diameter of 150 μm, for rutile with ~50 ppm Hf, the ^{176}Hf/^{177}Hf error is 0.0002, while for rutile with >100 ppm Hf, the ^{176}Hf/^{177}Hf error is below 0.0001. With the development of technology, it can be convinced that the requirement of accurate Hf isotope analysis will decrease gradually in the future. In summary, for most rutile (Hf content ~50 ppm), we can obtain high-qualified Hf isotopic results with current analytical procedure, which is proved in the following geological application.

4 Application

The Khondalite Belt located in the western block of the North China Craton is a suit of granulite facies metasediment consisting of felsic paragneiss, sillimanite-garnet-

Table 3 Lu-Hf isotopic composition of rutile U-Pb dating reference material

Sample	^{176}Yb/^{177}Hf	2SD	^{176}Lu/^{177}Hf	2SD	^{176}Hf/^{177}Hf	2SD (*n*=times)	Method	Source
JDX			0.000018	0.000004	0.281795	0.000015 (*n*=33)	Solution	This study
JDX	0.000200	0.000150	0.000009	0.000010	0.281796	0.000187 (*n*=89)	Laser	This study
R10			0.000029	0.000012	0.282199	0.000280 (*n*=3)	Laser	Ewing et al. (2011)
R10					0.282178	0.000012 (*n*=2)	Solution	Luvizotto et al. (2009)
R10	0.000379	0.000480	0.000026	0.000081	0.282157	0.000204 (*n*=42)	Laser	This study
Sugluk-4	0.000080	0.000392	0.000003	0.000016	0.281172	0.000107 (*n*=15)	Laser	This study
PCA-S207	0.000647	0.001668	0.000019	0.000049	0.281246	0.000146 (*n*=15)	Laser	This study

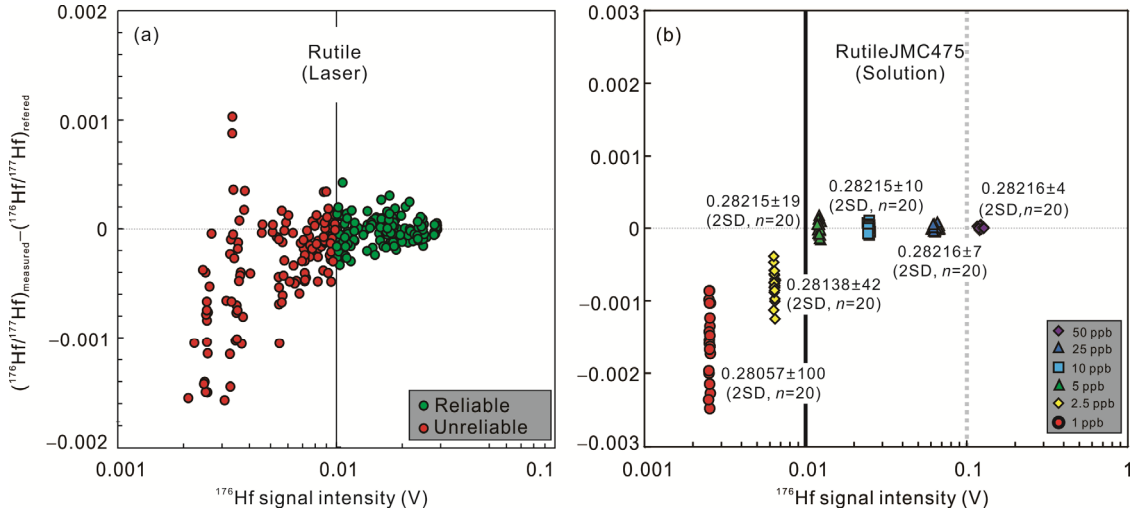

Figure 9 The test of experimental condition for acquiring accurate Hf isotope value in rutile by LA-MC-ICP-MS.

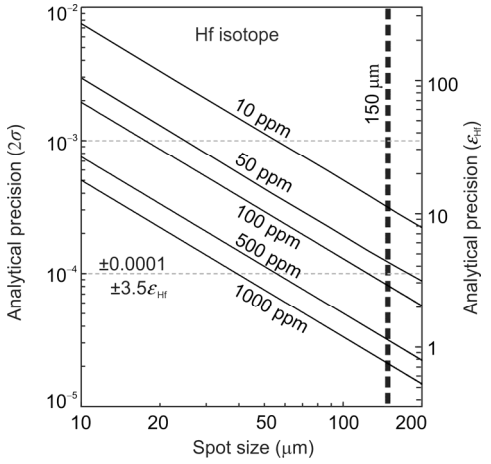

Figure 10 The relationship between precision of rutile Hf isotope analytical data, the laser spot size and Hf content.

plagioclase (K-feldspar or monzonitic) gneiss, arkosite, marble and calc-silicate rocks in association with small amount of mafic granulites, TTG gneisses and S-type granites (Lu et al., 1992, 1996; Zhao et al., 1999, 2005). The Khondalite Belt trends northwest and extends over 1000 km, and divided into three terranes from west to east. These are Helanshan-Qianlishan, Ulashan-Daqingshan and Jining-Liangcheng-Fengzhen (Figure 11). It is generally accepted that the Khondalite Belt is formed by amalgamation between the Yinshan Block in the north and the Ordos Block in the south at ca. 1.95 Ga (Zhao et al., 2003, 2005; Zhao, 2009), and it is deposited at ca. 1.95 to 2.00 Ga (Xia et al., 2006, 2008; Wan et al., 2006, 2009). According to detrital zircon U-Pb ages, two episodes (1.97 to 1.94 and 1.87 to 1.82 Ga) of metamorphic activity are recorded in the Khondalite Belt (Yin et al., 2009, 2011; Zhao et al., 2010; Li et al., 2011; Dong et al., 2013; Ma et al., 2012; Liu et al., 2013; Jiao et al., 2013). The 1.97 to 1.94 Ga metamorphic event may be connected with collision between the Yinshan Block and Ordos Block, while 1.87 to 1.82 Ga metamorphic event may be related with amalgamation of the Eastern Block and Western Block, or represents post-orogenic extension (Zhao et al., 2005, 2012; Jiao et al., 2013; Peng et al., 2014). In addition, 1.92 to 1.91 Ga ultrahigh temperature granulite has been identified in this region and is proposed to be concerned with the high-heat flow brought up by the injection of mantle magma (Santosh et al., 2007, 2009; Guo et al., 2012).

We analyze U-Pb ages and Hf isotopic compositions of zircon and rutile collected from granulite in Daqingshan and Jining terranes (Figure 12, Table 4). It is considered that the metapelitc granulites in both regions have experienced high to ultrahigh temperature metamorphism, and some samples even contain sapphirine (Jiao and Guo, 2011; Jiao et al., 2011). To ensure the reliability of *in situ* laser ablation Hf isotope analytical results in rutile, we measure their Hf isotope by solution method, which is consistent with the laser results, indicating our laser results are convincing.

In general, compared with zircon, the Hf isotopic compositions of rutile are relatively homogeneous in this region, and rutile has much lower $^{176}Lu/^{177}Hf$ ratio (Figure 13), suggesting massive garnet (rich in HREE) crystallization during the closure of Lu-Hf isotopic system of rutile.

Three rutile samples from the Dongpo outcrop in the

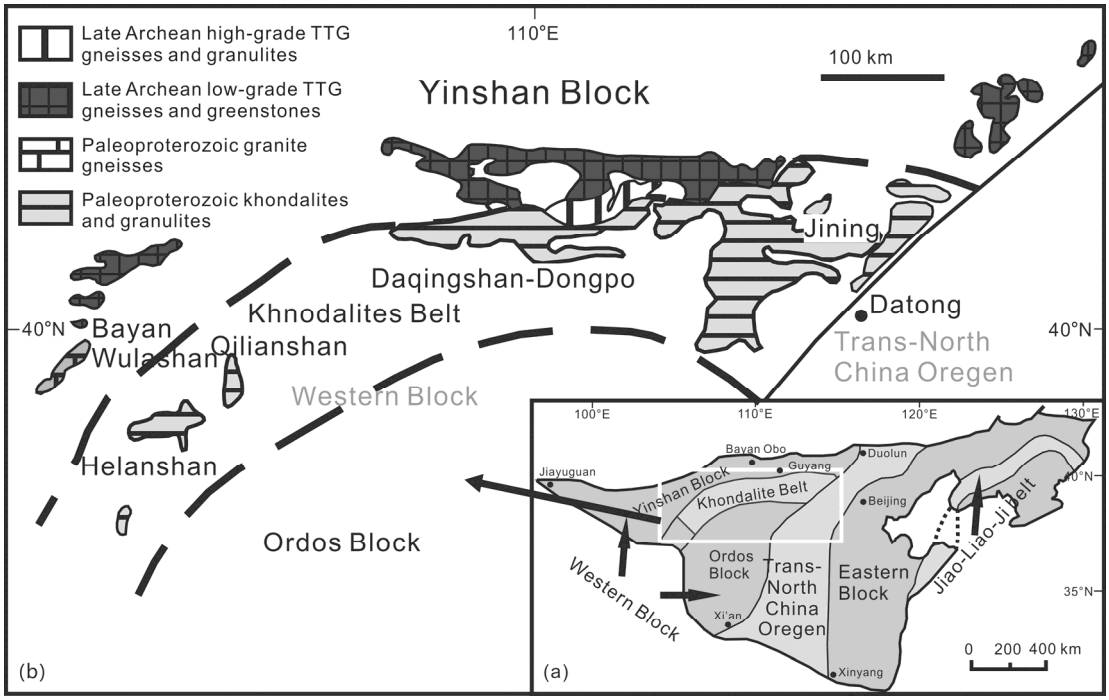

Figure 11 Tectonic subdivision of the North China Craton (a) and the Khondalite Belt within the Western Block (b) (modified from Dan et al. (2012)).

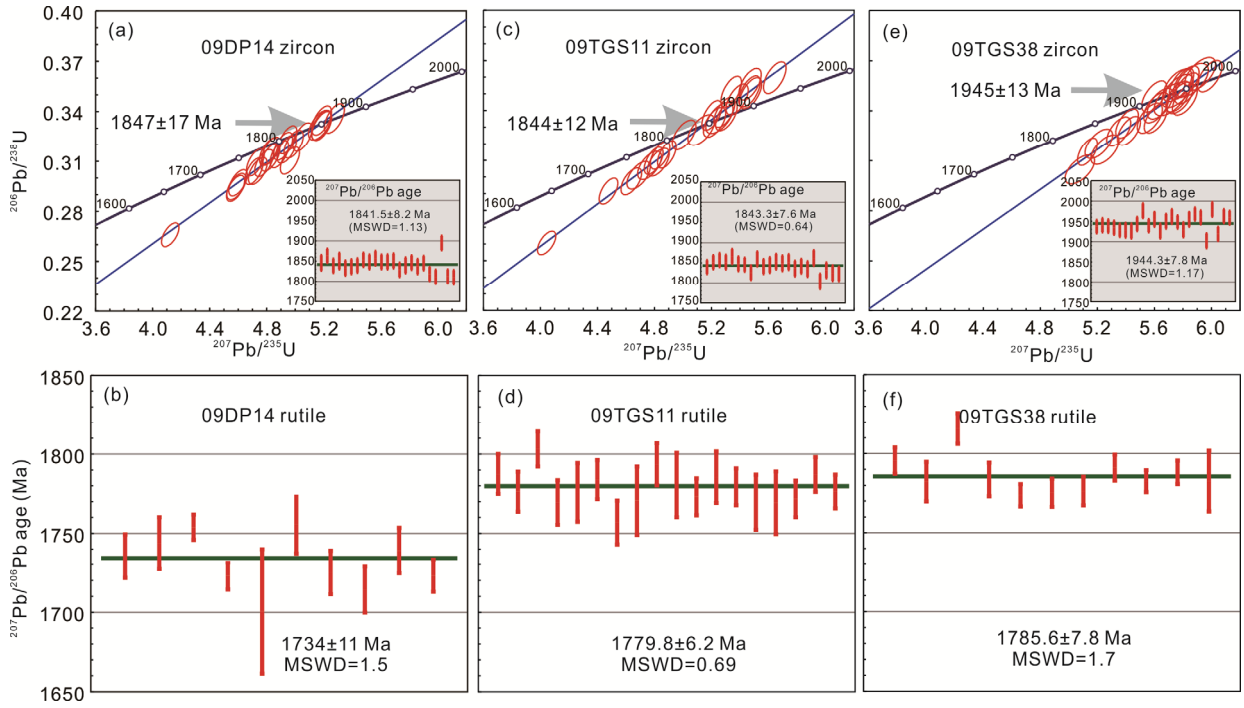

Figure 12 The SIMS U-Pb ages of zircon and rutile from the Khondalite Belt of the North China Craton.

Table 4 The U-Pb ages and Hf isotopic composition of zircon and rutile from Khondalite Belt in western block of North China Craton

Sample	Mineral	Ages (Ma)	^{176}Yb/^{177}Hf	^{176}Lu/^{177}Hf	^{176}Hf/^{177}Hf	2SE (n=times)	ε_{Hf} (1780)	2σ	Method
Daqingshan-Dongpo region									
09DP14	zircon	1842±8	0.00067	0.000021	0.281474	0.000009 (n=16)	−6.28	0.45	Laser
	rutile	1734±11	0.00000	0.000000	0.281531	0.000014 (n=15)	−4.23	0.70	Laser
	rutile				0.281539	0.000003 (n=7)			Solution
08JDP05	rutile		0.00029	0.000001	0.281560	0.000036 (n=4)	−3.20	1.30	Laser
	rutile				0.281555	0.000005 (n=2)			Solution
08JDP06	rutile		0.00070	0.000004	0.281541	0.000047 (n=2)	−3.88	1.68	Laser
	rutile				0.281554	0.000010 (n=2)			Solution
Jining-Tuguiwula region									
09TGS11	zircon	1843±8	0.00081	0.000023	0.281484	0.000008 (n=16)	−5.93	0.50	Laser
	rutile	1780±6	0.00011	0.000003	0.281593	0.000015 (n=15)	−2.03	0.60	Laser
	rutile				0.281591	0.000011 (n=4)			Solution
09TGS38	zircon	1944±8	0.00068	0.000020	0.281580	0.000010 (n=16)	−2.51	0.65	Laser
	rutile	1783±5	0.00003	0.000002	0.281598	0.000012 (n=15)	−1.85	0.48	Laser
	rutile				0.281605	0.000008 (n=7)			Solution
08TG13	rutile		0.00001	0.000001	0.281600	0.000014 (n=15)	−1.78	0.55	Laser
	rutile				0.281602	0.000009 (n=4)			Solution
08TPS01	rutile		0.00003	0.000000	0.281597	0.000012 (n=15)	−1.89	0.48	Laser
	rutile				0.281597	0.000015 (n=4)			Solution

Daqingshan terrain give nearly coincident ^{176}Hf/^{177}Hf values, whereas, the rutile in 09DP14 (sillimanite-garnet gneiss) give a weighted mean ^{207}Pb/^{206}Pb age of 1734±11 Ma, which is notably younger than its zircon age of 1841.5±8.2 Ma, confirming the closure temperature of U-Pb system in rutile is lower than that in zircon. If their ages are normalized to 1780 Ma, their Hf isotopic compositions are not in good agreement with each other.

Similar to rutile from the Daqingshan terrain, four rutile samples collected from the Tuguiwula outcrop in the Jining terrain give homogeneous Hf isotopic composition (slightly higher than rutile from the Daqingshan terrain). It is notable that rutile from 09TGS11 and 09TGS38 (both are sillimanite-garnet gneisses) give coincident ^{207}Pb/^{206}Pb ages (~1780 Ma), though zircon from these two samples give different ^{207}Pb/^{206}Pb ages (1843.3±7.6 Ma for 09TGS11 and 1944.3±7.8 Ma for 09TGS38). The 09TGS38 has a metamorphic age of ~1.94 Ga, and similar Hf isotopic composi-

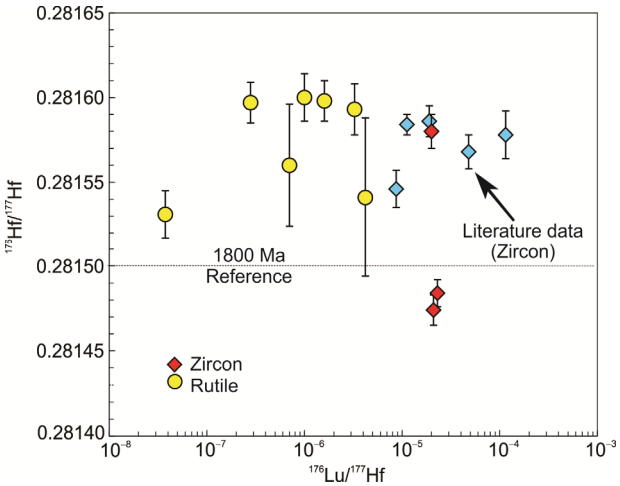

Figure 13 Lu-Hf isotopic composition of zircon (red diamond) and rutile (yellow circle) from Khondalite Belt in western block of North China Craton. Zircon data (blue diamond) are from Santosh et al. (2009) and Yang et al. (2014).

tion between zircon and rutile implies that the Hf isotopic system of rutile is not disturbed by later metamorphic event and its initial Hf isotopic signatures are preserved. As for 09TGS11, its $^{176}Hf/^{177}Hf$ value of rutile is obviously higher than that of zircon, and we propose the Hf source of rutile during crystallization process is different from that of zircon.

However, taking all published literature and data into consideration (Figure 13), it can be discovered that the Hf isotopic composition of zircon and rutile from older (~1.92 Ga) ultrahigh temperature granulite are generally the same, yet that from younger granulite exhibit notable differences. Consequently, the evolution history of the Khondalite Belt in the North China Craton is quite complicated and worth further investigation.

5 Conclusion

We analyzed Hf isotopic composition of rutile U-Pb reference materials (JDX, R10, Sugluk-4 and PCA-S207), which is consistent with solution results or literature data, suggesting that for rutile with low Hf content (~50 ppm), we can obtain reliable $^{176}Hf/^{177}Hf$ value with adequate precision for geological application. During analysis, the matrix-matched standard is necessary, which means zircon or other minerals cannot be used as standard for *in situ* rutile Hf isotope measurement. The key for acquiring accurate Hf isotopic composition in rutile is ensuring ^{176}Hf signal intensity above 10 mV, thus spot with larger diameter is needed. Based on the analytical procedure presented above, we analyzed Hf isotopic composition of rutile and zircon from the metapelitic granulites in different regions in Khondalite Belt of the North China Craton, and the results indicate that local granulite has experienced a complex metamorphic evolution history.

This research was supported by the National Natural Science Foundation of China (Grants Nos. 41130313 & 41525012). We thank Prof. Li Qiuli (IGGCAS) and Dr. Laura Bracciali (BGS) for supplying rutile U-Pb reference materials. We are grateful to Prof. Xu Cheng (PKU) for providing Lu spike. Anonymous reviewers are thanked for thorough reviews and amendments that significantly improved the manuscript.

Aulbach S, O'Reilly S Y, Griffin W L, Pearson N J. 2008. Subcontinental lithospheric mantle origin of high niobium/tantalum ratios in eclogites. Nat Geosci, 1: 468–472

Bracciali L, Parrish R R, Horstwood M S A, Condon D J, Najman Y. 2013. U-Pb LA-(MC)-ICP-MS dating of rutile: New reference materials and applications to sedimentary provenance. Chem Geol, 347: 82–101

Cherniak D J, Manchester J, Watson E B. 2007. Zr and Hf diffusion in rutile. Earth Planet Sci Lett, 261: 267–279

Choukroun M, O'Reilly S Y, Griffin W L, Pearson N J, Dawson J B. 2005. Hf isotopes of MARID (mica-amphibole-rutile-ilmenite-diopside) rutile trace metasomatic processes in the lithospheric mantle. Geology, 33: 45–48

Dan W, Li X H, Guo J H, Liu Y, Wang X C. 2012. Integrated *in situ* zircon U-Pb age and Hf-O isotopes for the Helanshan khondalites in North China Craton: Juvenile crustal materials deposited in active or passive continental margin? Precambrian Res, 222-223: 143–158

Dong C Y, Wan Y S, Xu Z Y, Liu D Y, Yang Z S, Ma M Z, Xie H Q. 2013. SHRIMP zircon U-Pb dating of late Paleoproterozoic khondalites in the Daqing Mountains area on the North China Craton. Sci China Earth Sci, 56: 115–125

Ewing T A, Rubatto D, Eggins S M, Hermann J. 2011. *In situ* measurement of hafnium isotopes in rutile by LA-MC-ICPMS: Protocol and applications. Chem Geol, 281: 72–82

Ewing T A, Hermann J, Rubatto D. 2013. The robustness of the Zr-in-rutile and Ti-in-zircon thermometers during high-temperature metamorphism (Ivrea-Verbano Zone, northern Italy). Contrib Mineral Petrol, 165: 757–779

Ewing T A, Rubatto D, Hermann J. 2014. Hafnium isotopes and Zr/Hf of rutile and zircon from lower crustal metapelites (Ivrea-Verbano Zone, Italy): Implications for chemical differentiation of the crust. Earth Planet Sci Lett, 389: 106–118

Ferry J M, Watson E B. 2007. New thermodynamic models and revised calibrations for the Ti-in-zircon and Zr-in-rutile thermometers. Contrib Mineral Petrol, 154: 429–437

Guo J H, Peng P, Chen Y, Jiao S J, Windley B F. 2012. UHT sapphirine granulite metamorphism at 1.93–1.92 Ga caused by gabbronorite intrusions: Implications for tectonic evolution of the northern margin of the North China Craton. Precambrian Res, 222-223: 124–142

Hu Z C, Liu Y S, Gao S, Liu W G, Zhang W, Tong X R, Lin L, Zong K Q, Li M, Chen H H, Zhou L, Yang L. 2012. Improved *in situ* Hf isotope ratio analysis of zircon using newly designed X skimmer cone and jet sample cone in combination with the addition of nitrogen by laser ablation multiple collector ICP-MS. J Anal Atom Spectrom, 27: 1391–1399

Jiao S J, Guo J H. 2011. Application of the two-feldspar geothermometer to ultrahigh-temperature (UHT) rocks in the Khondalite belt, North China Craton and its implications. Am Mineral, 96: 250–260

Jiao S J, Guo J H, Mao Q, Zhao R F. 2011. Application of Zr-in-rutile thermometry: A case study from ultrahigh-temperature granulites of the Khondalite belt, North China Craton. Contrib Mineral Petrol, 162: 379–393

Jiao S J, Guo J H, Harley S L, Peng P. 2013. Geochronology and trace element geochemistry of zircon, monazite and garnet from the garnetite and/or associated other high-grade rocks: Implications for Palaeoproterozoic tectonothermal evolution of the Khondalite Belt, North China Craton. Precambrian Res, 237: 78–100

Li Q L, Lin W, Su W, Li X H, Shi Y H, Liu Y, Tang G Q. 2011. SIMS U-Pb rutile age of low-temperature eclogites from southwestern Chinese Tianshan, NW China. Lithos, 122: 76–86

Li Q L, Yang Y N, Shi Y H, Lin W. 2013. Eclogite rutile U-Pb dating: Constraint for formation and evolution of continental collisional orogen. Chin Sci Bull, 58: 2279–2284

Li X P, Yang Z Y, Zhao G C, Grapes R, Guo J H. 2011. Geochronology of khondalite-series rocks of the Jining Complex: Confirmation of depositional age and tectonometamorphic evolution of the North China Craton. Int Geol Rev, 53: 1194–1211

Liu S J, Dong C Y, Xu Z Y, Santosh M, Ma M Z, Xie H Q, Liu D Y, Wan Y S. 2013. Palaeoproterozoic episodic magmatism and high-grade metamorphism in the North China Craton: Evidence from SHRIMP zircon dating of magmatic suites in the Daqingshan area. Geol J, 48: 429–455

Lu L Z, Jin S Q, Xu X C, Liu F L. 1992. Petrogenesis and Mineralization of Khondalite Series in the Southeastern Inner Mongolia. Changchun: Jilin Science and Technology Press

Lu L Z, Xu X C, Liu F L. 1996. Khondalite Series in Precambrian, North China. Changchun: Changchun Publishing House

Luvizotto G L, Zack T, Meyer H P, Ludwig T, Triebold S, Kronz A, Münker C, Stockli D F, Prowatke S, Klemme S, Jacob D E, von Eynatten H. 2009. Rutile crystals as potential trace element and isotope mineral standards for microanalysis. Chem Geol, 261: 346–369

Ma M Z, Wan Y S, Santosh M, Xu Z Y, Xie H Q, Dong C Y, Liu D Y, Guo C L. 2012. Decoding multiple tectonothermal events in zircons from single rock samples: SHRIMP zircon U-Pb data from the late Neoarchean rocks of Daqingshan, North China Craton. Gondwana Res, 22: 810–827

Meinhold G. 2010. Rutile and its applications in earth sciences. Earth-Sci Rev, 102: 1–28

Morisset C E, Scoates J S, Weis D, Rahier A. 2014. Methodology and application of hafnium isotopes in ilmenite and rutile by MC-ICP-MS. Geostand Geoanal Res, 38: 159–176

Nowell G M, Kempton P D, Noble S R, Fitton J G, Saunders A D, Mahoney J J, Taylor R N. 1998. High precision Hf isotope measurements of MORB and OIB by thermal ionization mass spectrometry: Insight into the depleted mantle. Chem Geol, 149: 211–233

Peng P, Wang X P, Windley B F, Guo J H, Zhai M G, Li Y. 2014. Spatial distribution of ~1950–1800 Ma metamorphic events in the North China Craton: Implications for tectonic subdivision of the craton. Lithos, 202-203: 250–266

Santosh M, Wilde S A, Li J H. 2007. Timing of Paleoproterozoic ultrahigh-temperature metamorphism in the North China Craton: Evidence from SHRIMP U-Pb zircon geochronology. Precambrian Res, 159: 178–196

Santosh M, Wan Y S, Liu D Y, Dong C Y, Li J H. 2009. Anatomy of zircons from an ultrahot orogen: The amalgamation of the North China Craton within the Supercontinent Columbia. J Geol, 117: 429–443

Thirlwall M F, Walder A J. 1995. *In situ* hafnium isotope ratio analysis of zircon by inductively coupled plasma multiple collector mass spectrometry. Chem Geol, 122: 241–247

Thirlwall M F, Anczkiewicz R. 2004. Multidynamic isotope ratio analysis using MC-ICP-MS and the causes of secular drift in Hf, Nd and Pb isotope ratios. Int J Mass Spectrom, 235: 59–81

Tomkins H S, Powell R, Ellis D J. 2007. The pressure dependence of the zirconium-in-rutile thermometer. J Metamorph Geol, 25: 703–713

Vry J K, Baker J A. 2006. LA-MC-ICPMS Pb-Pb dating of rutile from slowly cooled granulites: Confirmation of the high closure temperature for Pb diffusion in rutile. Geochim Cosmochim Acta, 70: 1807–1820

Wan Y S, Song B, Liu D Y, Wilde S A, Wu J S, Shi Y R, Yin X Y, Zhou H Y. 2006. SHRIMP U-Pb zircon geochronology of Palaeoproterozoic metasedimentary rocks in the North China Craton: Evidence for a major Late Palaeoproterozoic tectonothermal event. Precambrian Res, 149: 249–271

Wan Y S, Liu D Y, Dong C Y, Xu Z Y, Wang Z J, Wilde S A, Liu Z H, Yang Z S, Zhou H Y. 2009. The Precambrian Khondalite Belt in the Daqingshan area, North China Craton: Evidence for multiple metamorphic events in the Palaeoproterozoic era. Geol Soc Spec Publ, 323: 73–97

Watson E B, Wark D A, Thomas J B. 2006. Crystallization thermometers for zircon and rutile. Contrib Mineral Petrol, 151: 413–433

Wu F Y, Yang Y H, Xie L W, Yang J H, Xu P. 2006. Hf isotopic compositions of the standard zircons and baddeleyites used in U-Pb geochronology. Chem Geol, 234: 105–126

Xia X P, Sun M, Zhao G C, Luo Y. 2006. LA-ICP-MS U-Pb geochronology of detrital zircons from the Jining Complex, North China Craton and its tectonic significance. Precambrian Res, 144: 199–212

Xia X P, Sun M, Zhao G C, Wu F Y, Xu P, Zhang J, He Y H. 2008. Paleoproterozoic crustal growth in the Western Block of the North China Craton: Evidence from detrital zircon Hf and whole rock Sr-Nd isotopic compositions of the Khondalites from the Jining Complex. Am J Sci, 308: 304–327

Xie L W, Zhang Y B, Zhang H H, Sun J F, Wu F Y. 2008. *In situ* simultaneous determination of trace elements, U-Pb and Lu-Hf isotopes in zircon and baddeleyite. Chin Sci Bull, 53: 1565–1573

Yang Q Y, Santosh M, Tsunogae T. 2014. Ultrahigh-temperature metamorphism under isobaric heating: New evidence from the North China Craton. J Asian Earth Sci, 95: 2–16

Yang Y H, Zhang H F, Chu Z Y, Xie L W, Wu F Y. 2010. Combined chemical separation of Lu, Hf, Rb, Sr, Sm and Nd from a single rock digest and precise and accurate isotope determinations of Lu-Hf, Rb-Sr, and Sm-Nd isotope systems using Multi-Collector ICP-MS and TIMS. Int J Mass Spectrom, 290: 120–126

Yin C Q, Zhao G C, Sun M, Xia X P, Wei C J, Zhou X W, Leung W. 2009. LA-ICP-MS U-Pb zircon ages of the Qianlishan Complex: Constrains on the evolution of the Khondalite Belt in the Western Block of the North China Craton. Precambrian Res, 174: 78–94

Yin C Q, Zhao G C, Guo J H, Sun M, Xia X P, Zhou X W, Liu C H. 2011. U-Pb and Hf isotopic study of zircons of the Helanshan Complex: Constrains on the evolution of the Khondalite Belt in the Western Block of the North China Craton. Lithos, 122: 25–38

Yuan H L, Gao S, Dai M N, Zong C L, Günther D, Fontaine G H, Liu X M, Diwu C R. 2008. Simultaneous determinations of U-Pb age, Hf isotopes and trace element compositions of zircon by excimer laser-ablation quadrupole and multiple-collector ICP-MS. Chem Geol, 247: 100–118

Zack T, Kronz A, Foley S F, Rivers T. 2002. Trace element abundances in rutiles from eclogites and associated garnet mica schists. Chem Geol, 184: 97–122

Zack T, Moraes R, Kronz A. 2004a. Temperature dependence of Zr in rutile: Empirical calibration of a rutile thermometer. Contrib Mineral Petrol, 148: 471–488

Zack T, von Eynatten H, Kronz A. 2004b. Rutile geochemistry and its potential use in quantitative provenance studies. Sediment Geol, 171: 37–58

Zhao G C, Wilde S A, Cawood P A, Lu L Z. 1999. Tectonothermal history of the basement rocks in the western zone of the North China Craton and its tectonic implications. Tectonophysics, 310: 37–53

Zhao G C, Sun M, Wilde S A. 2003. Major tectonic units of the North China Craton and their Paleoproterozoic assembly. Sci China Ser D-Earth Sci, 46: 23–38

Zhao G C, Sun M, Wilde S A, Li S Z. 2005. Late Archean to Paleoproterozoic evolution of the North China Craton: Key issues revisited. Precambrian Res, 136: 177–202

Zhao G C. 2009. Metamorphic evolution of major tectonic units in the basement of the North China Craton: Key issue and discussion. Acta Petrol Sin, 25: 1772–1792

Zhao G C, Wilde S A, Guo J H, Cawood P A, Sun M, Li X P. 2010. Single zircon grains record two Paleoproterozoic collisional events in the North China Craton. Precambrian Res, 177: 266–276

Zhao G C, Cawood P A, Li S Z, Wilde S A, Sun M, Zhang J, He Y H, Yin C Q. 2012. Amalgamation of the North China Craton: Key issues and discussion. Precambrian Res, 222-223: 55–76